NTNU – Trondheim
Norwegian University of
Science and Technology

Pressure pulsations and stress in a high head turbine comparison between model and geometrically similar prototype.

Ingeborg Lassen Bue

Master of Science in Mechanical Engineering
Submission date: June 2013
Supervisor: Torbjørn Kristian Nielsen, EPT

Norwegian University of Science and Technology
Department of Energy and Process Engineering

NTNU
Norwegian University
of Science and Technology

Department of Energy
and Process Engineering

EPT-M-2013-28

MASTER THESIS

For
Stud.tech Ingeborg Lassen Bue

Spring 2013

Pressure pulsations and stress in a high head turbine – comparison between model and geometrically similar prototype.
Trykkpulsasoner i høytrykks Francisturbin – sammenligning mellom modell og prototype.

Background

In a hydro power plant, the turbines, due to the variation of the electric demand, will be running in different modes of operation outside the design performance point. Hence, the pressure pulsation amplitudes will vary and might give causes to fatigue.

A model of a high head Francis turbine will be installed in the Waterpower Laboratory at NTNU. The model is geometrical similar to an existing prototype turbine installed in a Norwegian power plant. The model is equipped with pressure transducers and strain gauges on one of the runner blades. For different performance, the pressure pulsations in the runner and draft tube shall be measured, as well as the stress on the runner blade.

The Master project shall be done in collaboration with Stud. tech Julie Marie Hovland

Objective

Establish relations between pressure pulsations measured in model and geometrically similar prototype

The following tasks are to be considered

1. The candidate shall participate in the installing the model turbine in the test rig and setting up the data acquisition system.
2. Learn how to run the laboratory
3. Evaluate the model laws and establish relations between model measured pressure pulsation and measurements in the prototype
4. Compare the measurements in the runner with the measurements in the prototype, considering the contributions from various phenomena (rotor-stator interaction, draft tube vortex, stochastic pulsations)
5. Based on model sigma variation, examine results for possible cavitation influence

Within 14 days of receiving the written text on the master thesis, the candidate shall submit a research plan for his project to the department.

When the thesis is evaluated, emphasis is put on processing of the results, and that they are presented in tabular and/or graphic form in a clear manner, and that they are analyzed carefully. The thesis should be formulated as a research report with summary both in English and Norwegian, conclusion, literature references, table of contents etc. During the preparation of the text, the candidate should make an effort to produce a well-structured and easily readable report. In order to ease the evaluation of the thesis, it is important that the cross-references are correct. In the making of the report, strong emphasis should be placed on both a thorough discussion of the results and an orderly presentation.

The candidate is requested to initiate and keep close contact with his/her academic supervisor(s) throughout the working period. The candidate must follow the rules and regulations of NTNU as well as passive directions given by the Department of Energy and Process Engineering.

Risk assessment of the candidate's work shall be carried out according to the department's procedures. The risk assessment must be documented and included as part of the final report. Events related to the candidate's work adversely affecting the health, safety or security, must be documented and included as part of the final report.

Pursuant to "Regulations concerning the supplementary provisions to the technology study program/Master of Science" at NTNU §20, the Department reserves the permission to utilize all the results and data for teaching and research purposes as well as in future publications.

The final report is to be submitted digitally in DAIM. An executive summary of the thesis including title, student's name, supervisor's name, year, department name, and NTNU's logo and name, shall be submitted to the department as a separate pdf file. Based on an agreement with the supervisor, the final report and other material and documents may be given to the supervisor in digital format.

☒ Work to be done in lab (Water power lab, Fluids engineering lab, Thermal engineering lab)
☐ Field work

Department of Energy and Process Engineering, 14.January 2013

Olav Bolland
Department Head

Torbjørn K. Nielsen
Academic Supervisor

Abstract

The aim if this Master's thesis was to establish relation between pressure pulsation amplitude in a model and a geometrical similar prototype. Model test has been conducted in the Water Power Laboratory at Norwegian University of Science and Technology (NTNU). The data collected from the model test has been compared with corresponding data from field measurements at the geometrical similar prototype. Three operation points have been compared; these were 42 %, 50 % and 75 % load. The comparisons were made from three different locations; draft tube cone, runner blade and vaneless space. As a scale-up relation the A/H fraction has been tested, but none of the pressure transducer showed a tendency to follow this relation.

Moreover it have been conducted pressure pulsation measurements on the model turbine for different sigma levels. These measurements were conducted at 50 % load with four different sigma levels with the range of 0.026 to 0.050. The sigma variation influence proved to be significant in the draft tube, and marginal in the runner. For the vaneless space the influence could be neglected. However the results from all the transducers showed a tendency of an increase in pressure pulsation amplitude with decrease in sigma level.

Sammendrag

Målet med denne masteroppgaven har vært å etablere et skaleringsforhold for trykkpulseringsamplituder mellom modell og en geometriske lik prototype. Modelltest har blitt gjennomført på Vannkraftlaboratoriet ved Norges teknisk-naturvitenskapelige universitet (NTNU). Data fra modelltesten har blitt sammenlignet med tilsvarende data fra feltmålinger på prototype. Tre driftspunkt har blitt sammenlignet, disse var 42 %, 50 % og 75 % last. Sammenligningene ble gjort fra tre forskjellige lokasjoner; sugerørskonus, løpehjulskovl og omdreiningshulrommet. Som oppskaleringsformel har A / H forholdet blitt testet. Ingen av trykktransduseren viste en tendens til å følge dette forhold.

Videre har det vært utført trykkpulseringsmålinger på modellturbinen for ulike sigmanivå. Disse målingene ble utført ved 50 % last hvor fire forskjellige sigmanivåer i området mellom 0,026 og 0,050 har blitt betraktet. Sigmavariasjonens innflytelse viste seg å være mest synlig i sugerørskonusen, og noe tilstede i løpehjulet. For omdreiningshulrommet kunne påvirkning neglisjeres. Resultatene fra transduserne viste en tendens til økning i trykkpulseringsamplitude ved reduksjon av sigmanivået.

Acknowledgment

This Master's Thesis has been written at the Water Power Laboratory in the department of Energy and Process engineering, Norwegian University of Science and Technology. It has been a practical Thesis where experiments in the laboratory have been central. The laboratory experience has taught me that experiments are time consuming. During the work we experienced troubles with many of different components which were central for completing the experiment. Looking back at the work I may say that I am happy for all the knowledge I gained through our trouble.

Without the helpful staff in the laboratory, the work would not have been possible to carry out. I would therefore thank Joar Grilstad, Bård Brandåstrø, Halvor Haukvik and Trygve Opland for their effort. Moreover I would like to thank Stein Kristian Skånøy for helping making the LabView program used for the data acquisition system.

I also want like to thank my supervisor Torbjørn Nielsen for guidance and sharing his experience during the work. Moreover I would like to thank Michel Cervantes for numerous Skype meetings where he has given advices when it comes to the set-up of the data acquisition system and much more. I also want to thank him for reading through and giving me feedback on my Master's Thesis.

Finally I would thank Julie Marie Hovland for great cooperation during all the work throughout the entire semester, and for all the fun we had when we have been working together.

_____

Ingeborg Lassen Bue

Table of contents

List of figures

List of tables

Abbreviations

BEP	Best Efficiency Point
FFT	Fast Fourier Transform
IEC	International Electrotechnical Commission
NTNU	Norwegian University of Science and Technology
NPSH	Net Positive Suction Head
RSI	Rotot Stator Interaction

List of symbols

Symbol	Description	Denomination
H	Head	[mWc]
Q	Flow	[m^3s^{-1}]
D	Diameter	[m]
A	Area	[m^2]
L	Length	[m]
n	Rotational speed	[rpm]
a	Speed of sound	[ms^{-1}]
g	Gravitation	[$m\ s^{-2}$]
f_n	Runner rotation frequency	[Hz]
f_{rb}	Runner blade passing frequency	[Hz]
f_{gv}	Guide vane passing frequency	[Hz]
f_{dt}	Draft tube vortex frequency	[Hz]
f_{wh}	Water hammer frequency	[Hz]
f_s	Logging frequency	[Hz]
f_m	Maximum frequency	[Hz]
h_b	Atmospheric pressue	[mWc]
h_{vd}	Evaporation pressue	[mWc]
z_{rb}	Number of runner blades	-
z_{gv}	Number of guide vanes	-
η	Efficiency	[%]
σ	Sigma level	-

1 Introduction

1.1 Background

Resent years there has been an increase of renewable energy sources connected to the grid. This gives a more unstable grid situation due to altering weather conditions which the renewables base their production on. Moreover maximization of the profit to the hydro power plants demands a wider range of operation. To compensate for the instability and sell at best price, hydro power plants have to operate at off design performance point. Most hydro power plants were constructed before the marked based operation was put in action, thus they were constructed to operate at the design performance point. Nowadays when turbines often are run with the objective to maximize the profit, problems arise considering wear and tear.

Pressure pulsations has proven to be more important when turbines run outside the best efficiency point (BEP) which leads to wear and worst case fatigue and breakdown. Moreover continuously trying to increase the efficiency has resulted in turbine runners with high efficiency and slim runner blades. These blades are more fragile and more vulnerable to cracking when exposed to pressure pulsation [1]. Therefore it is desirable to have a scale-up relation from model to prototype so pressure pulsation can be predicted in a prototype after model test has been conducted.

1.2 Previous work

There have been done numerous investigations on pressure pulsation in Francis turbines. One of the first out was W.J. Rheingans. He published in 1940 “Power swing in hydroelectric plants” where he considered the draft tube vortex [2].

At which frequencies the pulsation occur are predicable, but the problem arises when it comes to prediction of the amplitude and scale-up relation from model to prototype. Doing experiments where comparison of the pressure pulsation in model and prototype is expensive in both money and time. It is also difficult to have equal extensive measurements on a prototype runner and a model runner. These kinds of measurement require alteration when pressure transducers are introduced on the runner blades.

On the subject of comparing pressure pulsation in model and prototype of high head Francis there has been done little investigation. Einar Kobro [1] did extensive work in his doctoral thesis where he conducted both model- and prototype measurements. Audun Tovslid [3] did research on this topic in his Master’s Thesis at NTNU where the aim was to establish relation between pressure pulsation in model and prototype. However he did not succeed in finding a correlation between model and prototype.

1.3 Objective

The objective of this Master's Thesis was firstly to establish a measurement chain in the Water Power Laboratory at Norwegian University of Science and Technology (NTNU). The chain would include pressure measurements on the turbine runner, vaneless space, draft tube cone, inlet, draft tube, generator torque and the angular velocity.

Secondly the aim was to establish relation between pressure pulsations measured in model and geometrical similar prototype Francis runner. The results from the model test would be compared to similar test results from field measurements performed by Einar Kobro in 2009 [1]. The objective was to identify a general scale up relation for the pressure amplitude. Moreover the cavitation influence at different sigma levels for the model would be examined.

2 Theoretical background

2.1 Sources of pressure pulsations

Pressure pulsation can be a problem in hydro power plants. The pulsations occur with different intensity and at various frequencies. The origin of the pulsations is non-uniform velocity flow. It can cause vibration in the system, noise and the wear of the mechanical components. Moreover the pulsation can come in resonance with vibration from other sources and can cause failure of key parts of the power plant. There are several know sources of pressure pulsation, and their frequency can easily be found analytically [4].

Runner rotational pressure pulsation is created when a given point on the runner passes a fixed point for every rotation. If the runner blade is smooth and rotates perfectly symmetrically, the amplitude of the pressure pulsation is low. On the other hand, if the runner is damaged or rotates unsymmetrically around its axis, the amplitude could be significant [5]. The frequency of the runner rotational pressure pulsation is defined in Equation 2.1.

$$f = \frac{n}{60} \qquad 2.1$$

Where: n is the rotational speed

Regarding the rotor-stator interaction (RSI) there are two common frequencies, the runner blade passing frequency and the guide vane passing frequency. The runner blade passing frequency is a pressure pulsation that is created every time a runner blade passes a guide vane. The frequency is defined by Equation 2.2. This pulsation will be dominant when the turbine runs at stable operation points [5]. The amplitude varies with the gap in the vaneless space, thus dependent on the angle of the guide vanes.

$$f_{rb} = f \cdot z_{rb} \qquad 2.2$$

Where: z_{rb} is the number of rotor blades

The other RSI pulsation is the guide vane passing frequency. It is created when the wake from the guide vane enters the runner (Figure 2.1). This pulsation only occurs in the runner, thus measured in this issued area [1]. The frequency is defined in Equation 2.3.

$$f_{gv} = f \cdot z_{gv} \qquad 2.3$$

Where: z_{gv} is the number of guide vanes

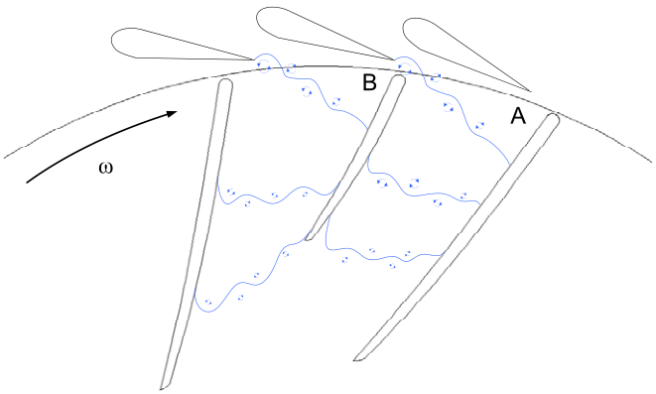

Figure 2.1 Guide vane wake in rotor **[1]**.

For both RSI pulsations it is evident that the amplitude decreases if the vaneless space increases. An increase of the vaneless space means an enlargement of the spiral casing and higher investment cost, and therefore the vaneless space is kept as small as possible [1].

Draft tube vortex frequency, also called the Rheingans frequency, is rotation of the masses due to the rotation of the system. It can be observed both upstream and downstream of the runner. At BEP the discharge flow is close to the parallel to the shaft, and the vortex is insignificant. If the load is lower than BEP, the vortex rotates with the same direction as the runner. While at load above BEP the direction of the vortex is opposite to the direction of the runner rotation [1].

The amplitudes of the swirling flow in the draft tube are small. First when a visible vortex is present, the amplitude is significant [1]. The visibility of the vortex is caused by cavitation. The pressure decreases below evaporation pressure, and vapor bubbles are created. Even though cavitation can be a serious problem when they implode, this is not necessarily a problem in the draft tube. The cavity vortex rope normally implodes before it reaches the walls of the draft tube, and thus is not harmful [1]. Cavitation is further discussed in chapter 2.2.

The frequency of the draft tube vortex is not defined exactly and varies for each case. As a general rule the frequency is defined by Equation 2.4 [5]. But frequency has been observed in the area defined by Equation 2.5:

$$f_{dt} = \frac{f}{3,6} \qquad 2.4$$

$$\frac{f}{f_{dt}} = 3.6 \pm 20\% \qquad 2.5$$

Other frequencies that can be present, especially during rapid changes in the wicket gates, are water hammer frequency and mass oscillation frequency. Water hammer occurs when the speed of change in the wicket gate is high enough to make the water behave elastically. The amplitude of the water hammer is dependent on the velocity of the wicket gate change. While the frequency of the water hammer is dependent on the speed of sound in the water. This is often defined to be 1200 ms^{-1} for channel flows; however it can vary in a wide range [6]. The frequency to the water hammer is defined in Equation 2.6, and the maximum amplitude is defined by Joukowsky`s equation (Equation 2.7), here written with the denomination meter water column (mWc) [6].

$$f_{wh} = \frac{a}{4L} \tag{2.6}$$

$$h = \frac{a\Delta c}{g} \tag{2.7}$$

Where: a is the speed of sound in water
L is the length of tunnel
c is the velocity of water
g is the gravitation

Mass oscillations may occur if the system has surge shafts. This oscillation has a low frequency (Equation 2.8). Equation 2.9 shows the amplitude dependency on the amount of water in the system and the time of change to the volume flow.

$$f_{mo} = \sqrt{\frac{g}{A_s \,/\, L / A_T}} \tag{2.8}$$

$$\Delta h = \Delta Q \sqrt{\frac{L / A_T}{g A_s}} \tag{2.9}$$

Where: Q is the volume flow
L is the length of tunnel between free surfaces
A_T is the cross section to the tunnel
A_S is the cross section to the surge shaft
g is the gravitation

2.2 Cavitation

Cavitation is a phenomenon that occurs when the pressure in the liquid decreases below the evaporation pressure of the liquid in question. Bubbles of vapor are created; most often this occurs on the solid surfaces. When the pressure rises beyond evaporation pressure, the bubbles implode and generate forces that can cause great damage due to erosion [7]. From the Bernoulli equation [8] it is evident that as the velocity increases the pressure decreases, thus areas with high velocity will be the areas where cavitation problem is most likely to occur. For a Francis turbine the draft tube is most exposed to cavitation [7].

To decrease the risk of cavitation, turbines are often submerged to increase the pressure in the draft tube. In fluid mechanics the Net Positive Suction Head (NPSH) (Equation 2.10) is defined and expresses the difference between the actual head pressure and evaporation pressure.

$$NPSH = -H_s + h_b + h_{va} \qquad 2.10$$

Where: H_s is the absolute distance from surface of tail water and center of turbine

h_b is atmospheric pressure

h_{va} is the evaporation pressure of water

Turbines are often designed with properties that require submergence, such demand is defines as the NPSH required ($NPSH_R$). For the available submergence at site $NPSH_A$ is defined. To meet the demand for secure operation $NPSH_R < NPSH_A$ need to be fulfilled [7].

2.3 Dimensional analysis and hydraulic similitude

There are different reasons why it is desired to perform model tests. Many cases are too complex to perform accurate results from analytical approach. Even computational fluid dynamic (CFD) models are often too expensive in computational memory to execute accurate data [8]. Another argument for doing model tests is if changes are requested. The aim of model test is to predict the behavior of a prototype, if the model test indicates that alterations are needed the cost of making changes is severely reduces in place of making the changes after the prototype is manufactured [9].

Dimensional analysis is based on comparison of dimensionless numbers. For hydro power this has been used to develop performance diagram for the turbine. The International Electrotechnical Commission (IEC) standard [10] has central guide lines for how to perform model tests. The IEC claim that there are two criteria which need to be met to achieve hydrodynamic similitude between model and prototype; geometrical similitude and equal ratio of forces. This is obtained if all the dimensionless numbers in question are equal. The most common factors are summarized in Table 2.1.

Table 2.1: Dimensionless numbers [8]

Formulae	Dimensional parameter	Description
$\mathrm{Re} = \frac{\rho v D}{\mu}$	Reynolds number	Describes the degree of turbulence. Important for free and non-free surface flow.
$Eu = \frac{p}{\rho v^2}$	Euler number	Is important if the pressure drops to a level where cavitation might occur.
$W\mathrm{e} = \frac{L v^2 \rho}{\gamma}$	Weber number	Weber number is only of importance if it is less than one. Meaning that the surface curvature is in same order as the depth of the fluid.
$Fr = \frac{v^2}{gD}$	Froude number	Expresses the similarity between the stationary inertia and the mass when it is limited to the force of gravity. Only of importance for free-surface flow.
$Ma = \frac{v}{a}$	Mach number	Is of interest in compressible fluids with high velocities.

Where: ρ is the density
v is the velocity
D is the diameter
μ is the kinetic viscosity
P is the pressure
L is the characteristic length

g is the gravitational force
ε is the roughness
γ is the surface tension
a is the speed of sound

Unfortunately it is not achievable to have all the factors similar at once. According to the IEC [10] one should only take in account the factors with the most influence. The IEC concludes that a model turbine and a prototype turbine run at corresponding operation points if the discharge (Equation 2.11), speed factor (Equation 2.12) and Thoma number (Equation 2.13) are the same [10].

$$Q_{ED} = \frac{Q}{D^2\sqrt{gH}} \qquad 2.11$$

Where: Q is the flow
D is the diameter
g is the gravitational force
H is the head

$$n_{ED} = \frac{nD^2}{\sqrt{gH}} \qquad 2.12$$

Where: n is the rotational speed
D is the diameter
g is the gravitational force
H is the head

For comparison of the cavitation influence, NPSH is reduced to the dimensionless number σ by dividing each term by the reference head:

$$\sigma = \frac{NPSH}{H} = \frac{-H_s}{H} + \frac{h_b}{H} + \frac{h_{va}}{H} \qquad 2.13$$

Where: H_s is the difference in height from the center line of the runner to the tail water level.
h_b is the atmospheric pressure.
h_{va} is the evaporation pressure to water
H is the net head

Equation 2.13 indicates that when increasing the submergence of the turbine the σ-level increases, hence elevated σ-level is desired.

2.3.1 Scale-up relation for pressure pulsation amplitude

There has not been conducted many measurements where the aim has been to compare the pressure pulsations between model and prototype. It is expensive in both time and money, and can be difficult to carry out such measurements since it require on-board logging chain to observe the pulsations in the whole turbine [1].

The IEC has not defined a scale-up relation for pressure pulsation amplitude, so today the question of a scale up relation of pressure pulsation amplitude is yet to be defined. It is believed that it is difficult to obtain a scaled model setup that is completely similar to a prototype setup [9]. However it might be possible to find empirical formula if many measurements were conducted.

There is a theory that states that a scale-up for the amplitude can be defined as the amplitude divided by the reference head. This has not yet proven to be the case. Audun Tovslid [3] did a Buckingham PI theorem analysis in his Master's Thesis where it is stated that the amplitude is a function of:

$$A = f(\rho, \mu, D_1, D_2, H, n, a, Q, g) \qquad 2.14$$

The analysis resulted in:

$$\frac{A}{H} = f\left(\frac{D_1}{D_2}, Q_{ED}, Eu, Ma, n_{ED}, \mathrm{Re}\right) \qquad 2.15$$

Where: $$Q_{ED} = \frac{Q}{D^2\sqrt{gH}}$$

$$n_{ED} = \frac{nD^2}{\sqrt{gH}}$$

Thus the relation $\frac{A}{H}$ should be the same for model and prototype if all the dimensionless fractions are equal in Equation 2.15. This equality is difficult to obtain and is further discussed in chapter 3.1.2.

2.4 Signal processing

In digital data acquisition systems the sampled signal is a discrete time signal, while analog signal is continuous. Due to the discrete sampling data between each recorded point is lost. This can cause incorrect results if precautions are not taken.

The sampling rate has to be in accordance to the sampling-rate theorem (Equation 2.16). If this requirement is not met aliasing may occur [11]. Aliasing is a phenomenon which gives faulty results due to inadequate sampling. As shown in Figure 2.2 the aliasing signal has a longer period than the real signal and therefore gives a lower frequency signal that does not exist.

$$f_s > 2 f_m \qquad 2.16$$

Where: f_s is the sampling rate

f_m is the highest expected frequency

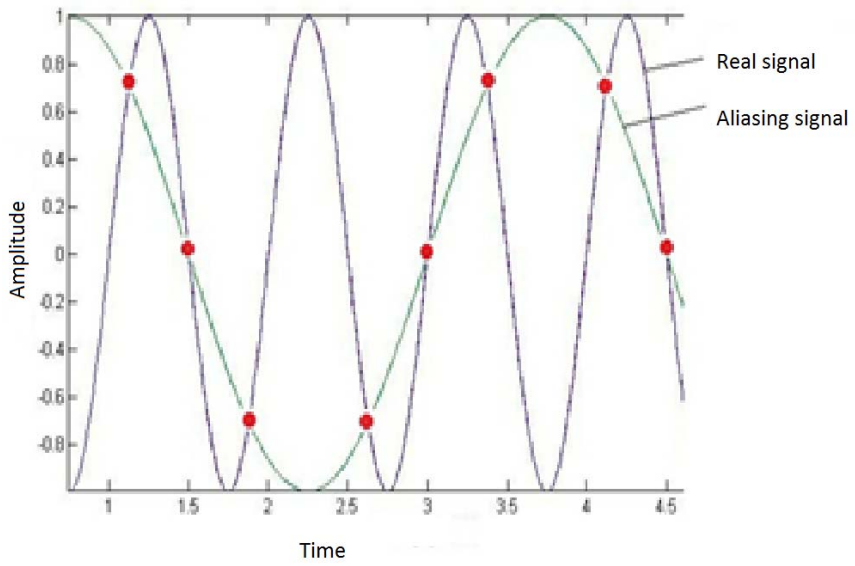

Figure 2.2: Effect of aliasing

To ensure that all frequencies in the output data are real, frequencies higher than twice the signal frequency can be neglected since it is known that these frequencies do not exist [11]. Signal with frequencies above the f_m will still be sampled by the acquisition system. To disregard these signals from the analysis, signal filtering needs to be implemented. What the filter does is to multiply the high frequencies with a factor lower than one, thus the amplitude will be severely decreased, and play an insignificant role in the final results [11].

Spectral analysis is often used to analyze sampled data. The spectral analysis transfers the signal into series of sine and cosine waves through the Fast Fourier Transform (FFT). This is used to transfer data from the time domain into the frequency domain. Since signals rarely

are pure sine or cosine waves, each signal consists of several waves with varying amplitudes and frequencies [11]. In Figure 2.3 this is demonstrated with a saw tooth wave that can be divided into two waves with different amplitude and frequencies. In the frequency plot the wave with the lower amplitude and higher frequency will show as a harmonic of the dominating frequency. The harmonics have frequencies that are a function of the first harmonic multiplied with an integer [11] (Figure 2.4).

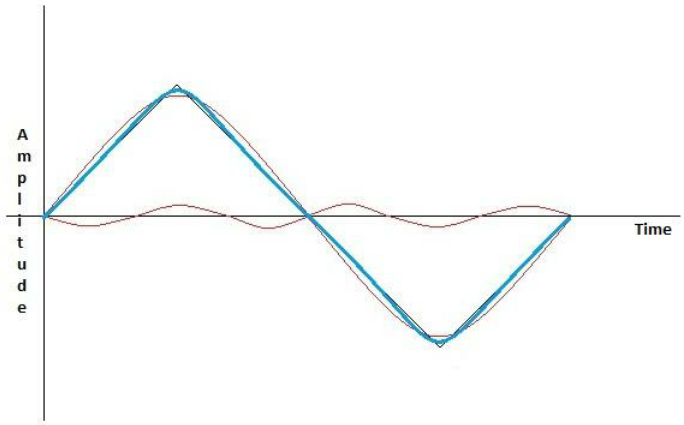

Figure 2.3: Wave form signal

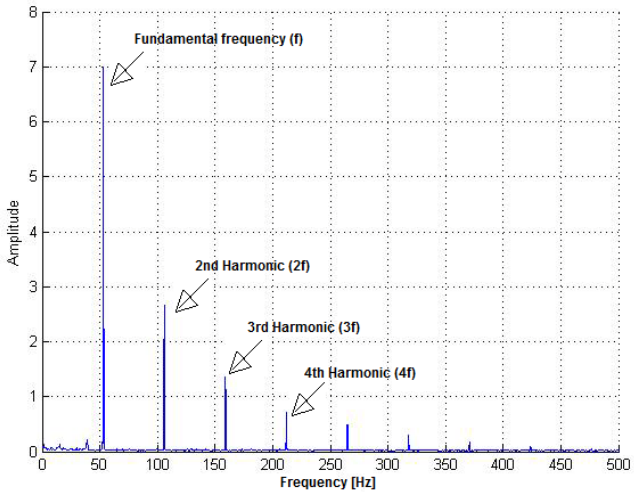

Figure 2.4: Harmonics in signal

At the beginning and the end of a sampling period there might be spectral leakage. This occurs because FFT assumes that every signal is periodic and infinite, which is not the case at the borders of the sampling interval. To reduce the leakage windowing is applied [12]. There are several ways of using windowing; in this thesis the Welsh method with Hanning window has been used. This method is illustrated in Figure 2.5. First the signal is divided into windows in the time domain; these windows are multiplied with a cosine variable which

dampens the signal at the borders of the windows. After this is applied the windows are shifted resulting in overlapping to get the signal reconstructed [12].

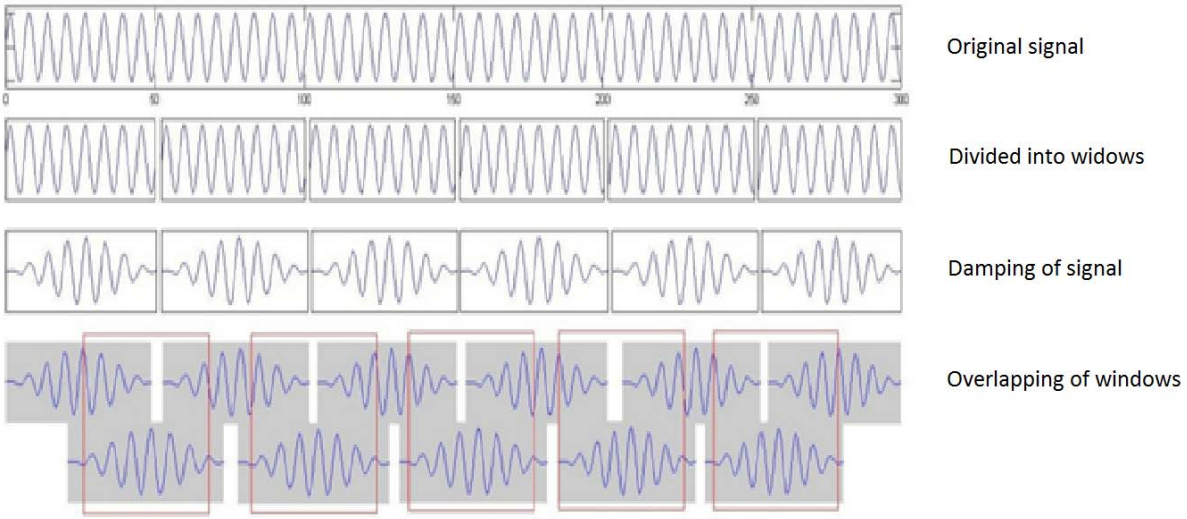

Figure 2.5: The Welsh method **[3]**

When using this method information might get lost if the signals are not pure sine or cosine waves. The result from the FFT will show the correct frequencies, but the amplitudes may have altered during the overlapping of windows. For measurement in hydraulic machinery this is often the case since pressure pulsations are not pure sine and cosine waves.

3 Methods

3.1 Model measurement

3.1.1 Setup in laboratory

The NTNU Water Power Laboratory facilitates a Francis rig that is constructed to enable model tests in both open and closed loop. For the pressure pulsation investigation in this thesis, the closed loop was used.

The closed loop consists of a pressure tank, turbine, draft tube tank and a pump as shown in Figure 3.1. The head for the loop is set by the rotational speed of the pump. In the draft tube tank there is a vacuum pump which regulates the submergence of the turbine.

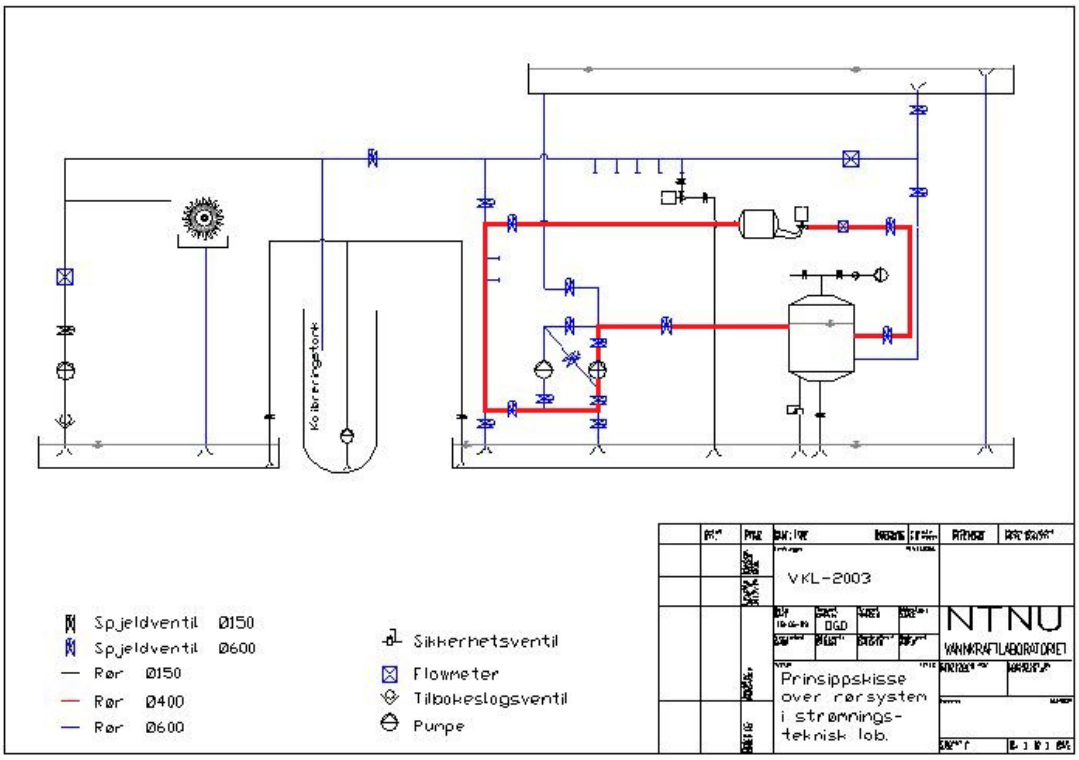

Figure 3.1: Sketch of the closed loop

The pressure pulsation measurements were conducted with numerous transducers in the loop. In Figure 3.2 these are presented with placement, type and quantity. There were two transducers in the inlet, respectively 4.77 m and 0.85 m from the spiral casing block. Three transducers were placed in the vaneless space, and three in the draft tube cone. Moreover there was one transducer just before the draft tube tank. Other measurements like generator torque and shaft position were also included in the data acquisition system.

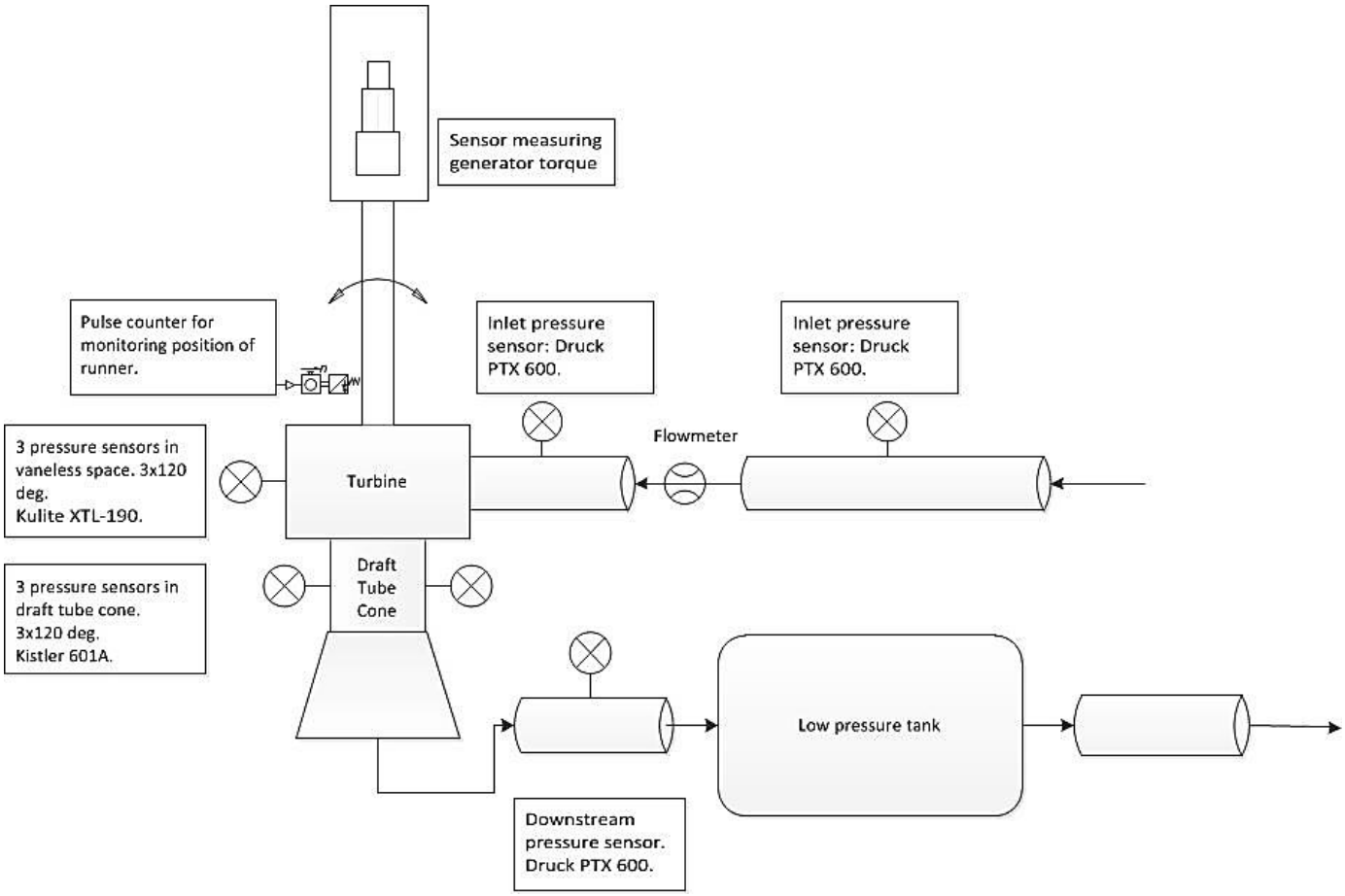

Figure 3.2: Data acquisition system

From the manufacture 18 pressure transducers were mounted on the runner. Nine were placed on the pressure side and nine on the suction side. They were placed so all the measurements were taken from one channel. The placements of the transducers are indicated in Figure 3.3. The type of transducers used on the runner was Kulite LL-080 with a pressure range of 17 bars.

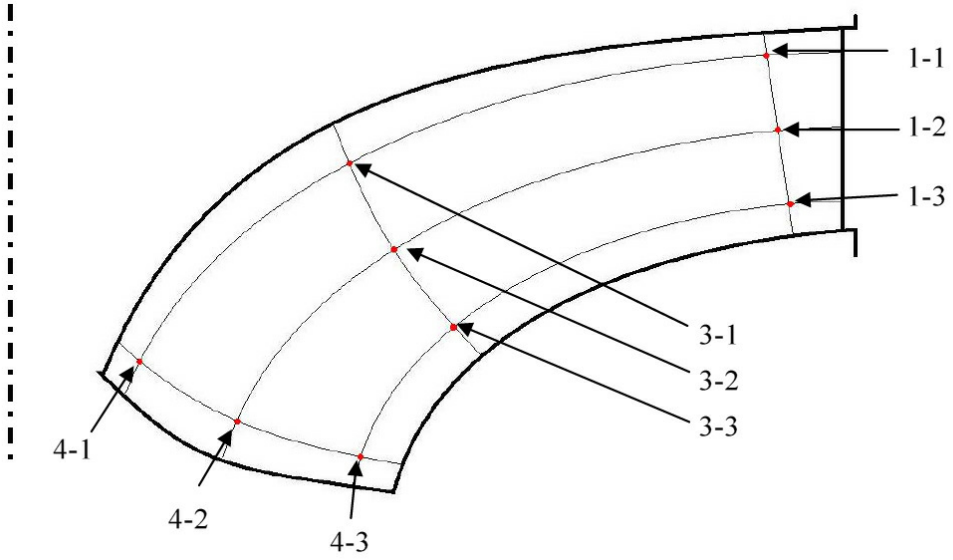

Figure 3.3: Locations of pressure transducers on model runner blade **[13]**

3.1.2 Dissimilarities between model and prototype

To obtain accurate results and to be able to compare data from model and prototype tests, all components have to have the same scale factor. Furthermore the dimensionless numbers in question (Equation 2.15) have to be equal. This is difficult to reach and there have been several dissimilarities between the model test and the prototype test in this experiment. In this chapter the dissimilarities for the setup has been presented.

When making hill diagram, tests are conducted with the model turbine, and the performance is recorded at given Q_{ED} and n_{ED}. If the model and the prototype are geometrically similar the efficiency will be alike. The problem arises when dynamic forces are included. From the definition of Reynolds number, it is evident that $\mathrm{Re}_{Prototype} >> \mathrm{Re}_{Model}$. When the Reynolds's number increases, the relative friction losses decrease, thus $\eta_{Prototype} > \eta_{Model}$. However the Moody diagram indicates that when the Reynolds number is high, the friction factor becomes constant for rough surfaces. Thus to ensure as accurate results as possible it is important to maintain high Reynolds number, and at least in the turbulent area. The IEC standard demands a minimal Reynolds number of $4 \cdot 10^6$ [10] for model tests.

Another problem arises when comparing the sigma level between the model and prototype. The atmospheric pressure is the same for both cases. Even though the draft tube tank is operated with a vacuum pump, this is only for adjusting the pressure head for the outlet of the runner and not for scaling of h_b. This means that the σ-level is correct for the center line in the turbine, but will differ in draft tube due to higher relative velocity in the model. If the test were to be conducted under scalable conditions, the whole rig would have to be constructed in a vacuum tank for reducing the ambient pressure for all components. The

latter term in the sigma equation (Equation 2.11), represent the evaporation pressure for water which is a constant property. To be able to adjust this term another fluid with the desired property would have to be used.

The speed of sound may vary in water due to pipe dimensions, material properties and the water quality [14]. When regarding hydro power plants the speed of sound is often defined as a constant of 1200 ms^{-1} [6]. To obtain better results the speed of sound should be measured in both model and prototype.

Frequencies that are connected to the construction may also occur in the frequency analysis. All the components such as piping system, inertia of generator and turbine should be relatively equal. Considering the piping system, diameter and length are most likely to be out of scale. Moreover the prototype normally has blasted tunnels with high roughness in comparison to the piping system to the model in the laboratory. Tests performed in the laboratory in 2012 by Anders Tørklep [15] showed frequencies that did not coincide with any expected frequency, these were suspected to be eigenfrequencies to the rig [3].

3.1.3 Data acquisition system

The data acquisition system was divided into two separate parts with one National Instruments CompactRIO-9074 (cRIO) connected to each system. Both were had an eight slot chassis. Each device was set up with a Field-programmable gate array (FPGA) which allows reprograming due to a silicon chip [16]. The programs were written in the Real-Time language. Both cRIOs were programmed to run in stand-alone mode, and a trigger button was connected to both cRIOs. This was triggered for every logging point.

The first cRIO was equipped with two NI9239 modules and one NI9237 module. Here data were logged from all the stationary transducers; vaneless space, generator torque, inlet pressure, the optical sensor that monitors the position of the shaft, draft tube cone and the transducer at the outlet.

The second cRIO had an eight slot chassis with five NI9237 modules and one NI9239 module. This cRIO was mounted on the rotating shaft and logged data from the transducers on the runner. The optical sensor was also connected to this cRIO to enable comparison between the two cRIOs and verify simultaneous logging. This was done by transferring the signal from the optical sensor via a slip ring on the shaft. Furthermore the slip ring provided power for the cRIO in addition to receive the trigging signal (Figure 3.4).

Figure 3.4: cRIO and slip rings mounted on shaft

The frequencies of the pressure pulsations can be found by using equations presented in chapter 2.1. This was the foundation for deciding the logging frequency in the data acquisition system. In accordance to the sampling rate theorem the logging frequency has to be at least twice the frequency of the highest expected frequency. This resulted in approximately 600 Hz. In the matter of logging frequencies 600 Hz is still a very low logging frequency. The cRIOs used had a minimum logging frequency of 1613 Hz. After checking the storage capacity of the cRIOs it was decided a logging frequency of 2000 Hz. This covers the sampling rate theorem with a good margin, moreover a high logging frequency provide better data resolution. To fulfill the requirements from the manufacturer of the turbine runner, the logging time for each measurement was set to 120 s.

3.1.4 Calibration

The turbine runner was already equipped with Kulite LL-080 pressure transducers from the manufacturer. These transducers needed to be calibrated in the laboratory before installation of the runner in the rig. The calibration was performed by placing the runner in a pressure tank which was connected with supply water and a manual pump (Figure 3.5). A reference pressure transducer was in addition connected to the pressure tank. All the wires from the transducers were led through a rubber cap to make the connection waterproof. The calibration was performed by logging all the transducers, inclusive the reference transducer, by first increasing and later decreasing the pressure with the manual pump. The results can be found in Appendix A.

There were also performed calibrations of the generator torque, inlet transducer, transducers in the vaneless space and draft tube transducers. All these reports can be found in Appendix A. The calibrations of the transducers in the draft tube cone were not conducted since they are of the piezoelectric type which only responds to dynamic pressure [1] and there was not equipment in the Water Power Laboratory to perform such calibration. Data from the manufacturer of the transducers were used.

Figure 3.5: Calibration tank

3.2 Prototype measurements

In 2009 Einar Kobro [1] performed field measurement on a geometrical similar prototype turbine. The aim of the tests was to investigate the development of static and dynamic pressure in the whole turbine. For doing this both strain and pressure transducers were mounted on a runner blade. In this Master's Thesis the emphasis has been on pressure pulsation, and data from strain measurements has been disregarded. The test had a rotating and a stationary logger as in the model test, thus it was possible to see the development of the pressure pulsation throughout the entire turbine [1].

On the prototype runner there were mounted pressure transducers at the inlet and the outlet of the runner blade. They were placed in the same relative position as the model runner. In Figure 3.6 the inlet transducers have been marked in grey, and the transducers at the outlet are marked in black. On the suction side there were three transducers at the inlet and three transducers at the outlet. While on the pressure side transducers were only mounted by the outlet. Due to problems with the pressure transducers at the inlet, no data was obtained from here [1]. In Table 3.1 brief data for the equipment used for the onboard field test has been presented.

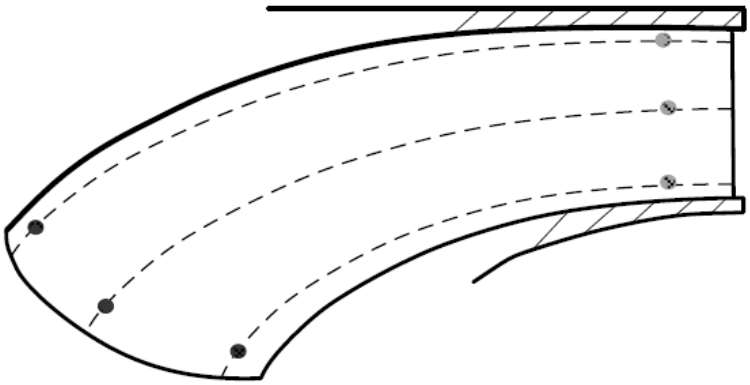

Figure 3.6: Location of pressure transducers on prototype runner blade **[1]**

Table 3.1: On board prototype logging equipment

Device	Description
Kistler Type 7031	Quartz pressure sensor -inlet of runner
Kulite LL080	Strain gauge based miniature pressure transducer -outlet of runner
National Instruments Compact Rio 9014 With eight slot chassis	Real Time controller
NI 9237	Strain gauge logging modules. -Six in the chassis
NI 9239	Logging module -One in the chassis

The stationary logging system had three pressure transducers in the rotational cavity. In addition there were two pressure transducers in the draft tube cone [1]. Available data for the equipment used in the stationary logging system has been listed in Table 3.2.

Table 3.2: Stationary prototype logging equipment

Device	Description	Placement
Kulite XTE 190	Pressure transducer	Rotational cavity
Druck PTX	Pressure transmitter	Draft tube cone

To ensure simultaneous logging for both the onboard and stationary systems, one common trigger button was used. Nevertheless there was a possibility that it could be a difference in milliseconds between the two logging systems. The tests were performed with a logging frequency of 1613 Hz, and the sampling time was 13.8 s for the rotating logging and 25 s for the stationary logging.

4 Results

4.1 Calibration of runner transducers

After the transducers were exposed to water during the calibration, several started to fail. When increasing the pressure water started to leak out through the wires (Figure 4.1) and more transducers failed. After the calibration the tank was emptied and the equipment dried, the transducers were checked and at this point only nine transducers proved to be functioning.

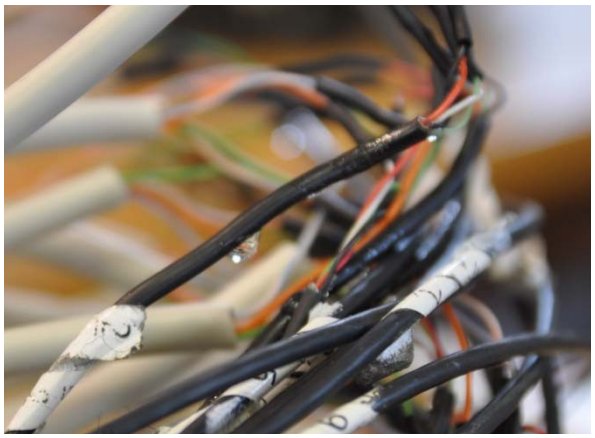

Figure 4.1 Leakage through wires

There were several pressure transducers which failed after contact with water in the prototype runner as well. In Figure 4.2 the corresponding pressure transducer which gave results for both model and prototype runner has been marked with a red circle.

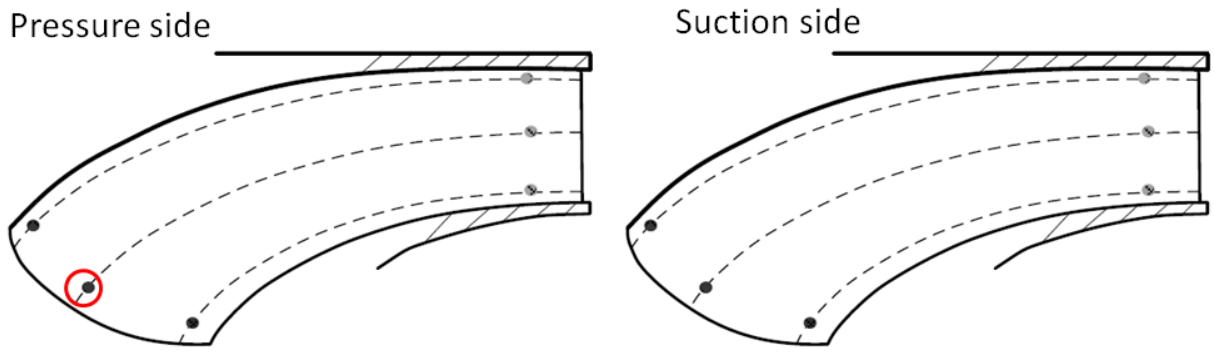

Figure 4.2: Corresponding functioning pressure transducers

4.2 Model testing results

All the logged operation points were performed at constant rotational speed which corresponds to the synchronic speed of prototype. The aim of the model measurements was to log pressure pulsation at same load and placement as in the prototype. Due to difficulties in the laboratory, time was limited and the extent was restricted. The chosen logged operation points were 42 %, 50 % and 75 % load. The chosen corresponding transducers were one from runner blade at pressure side, one from the vaneless space and one from the draft tube cone. In this chapter example graphs for the transducers in question at 50 % load have been presented. All the frequencies and pressure amplitudes has been normalized due to confidentiality. The graphs presented in this section have been the foundation for comparison of the amplitudes in section 4.4.

Table 4.1: Expected frequencies for model turbine

Pressure pulsation source	**Normalized frequency [-]**
Runner rotation frequency	1
Runner blade passing frequency	17
Guide vane passing frequency	28
Draft tube vortex frequency	0.2778

Testing of the system before the conduction of the planned logging section, it was suspected that air was sucked into the system when the pressure in the draft tube decreased. This was confirmed by videos from the high speed camera which filmed the draft tube cone. The air entered where the wires from the pressure transducers on the runner blade exit, and traveled inside the shaft and entered the draft tube through the O-ring under the hub. It was also validated by the fact that a visible vortex was present at operation points where drawings from the manufacturer indicated that there should not be a vortex. The hole in the shaft where the wires exited was clogged to prevent air entering the system (Figure 4.3).

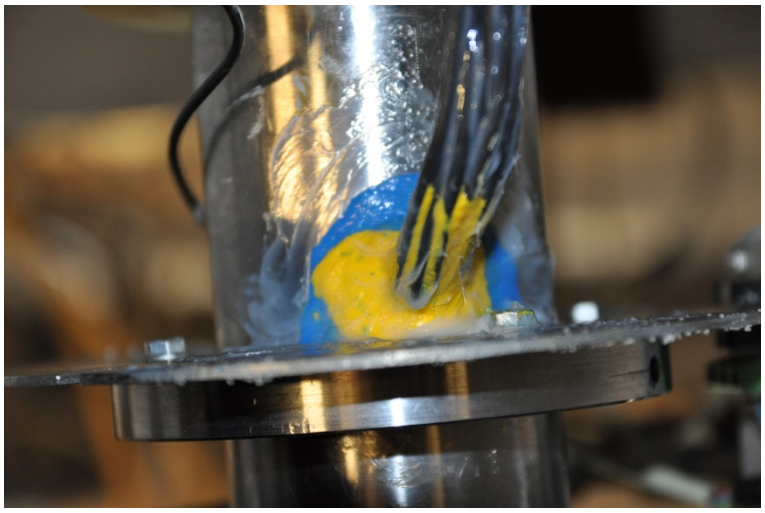

Figure 4.3: Clogging of the hole on the shaft where the wires from the runner transducers exit

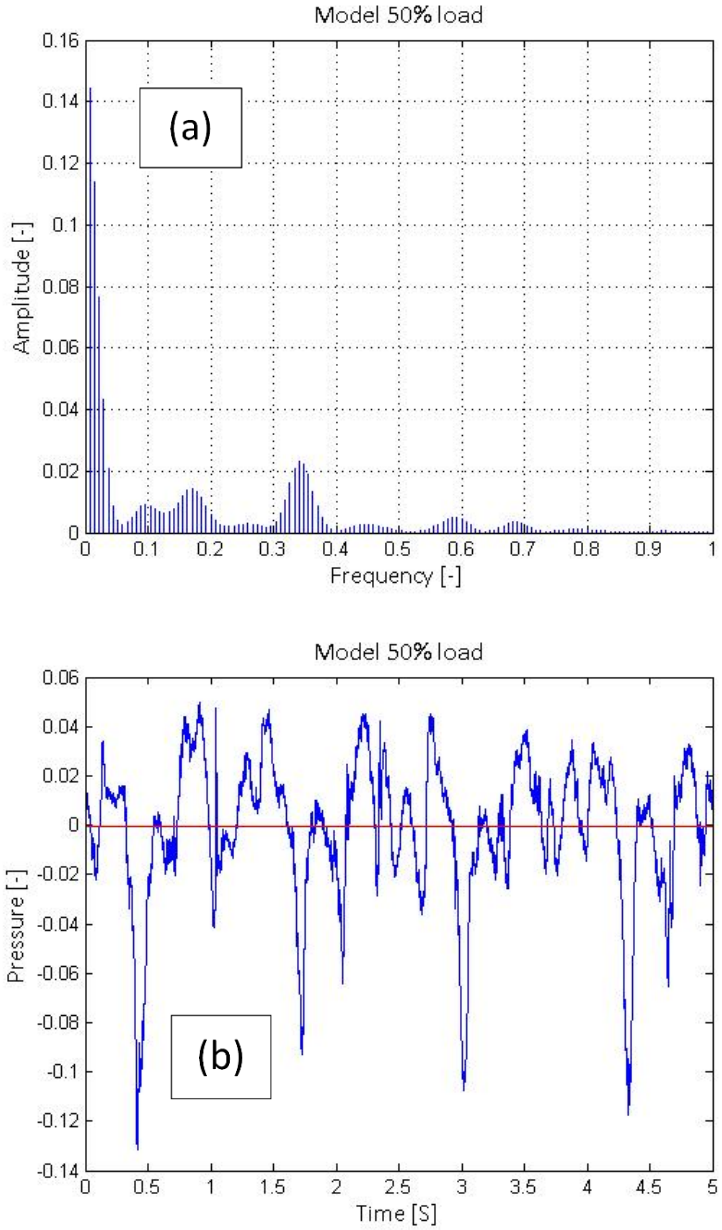

Figure 4.4: Frequency (a) and time (b) domain plot for model's pressure transducer in the draft tube cone (Figure 3.2)

The expected vortex in the draft tube had the normalized value of 0.2778. In Figure 4.4 this frequency was not identifiable. The frequency plot showed randomly distributed low frequencies.

It was suspected that air was still entering the system, and that the clogging of the hole on the shaft was not completely air proof. For comparison of the pressure amplitude with the prototype it was decided to use the mean of the dominating peaks from Figure 4.4 (b).

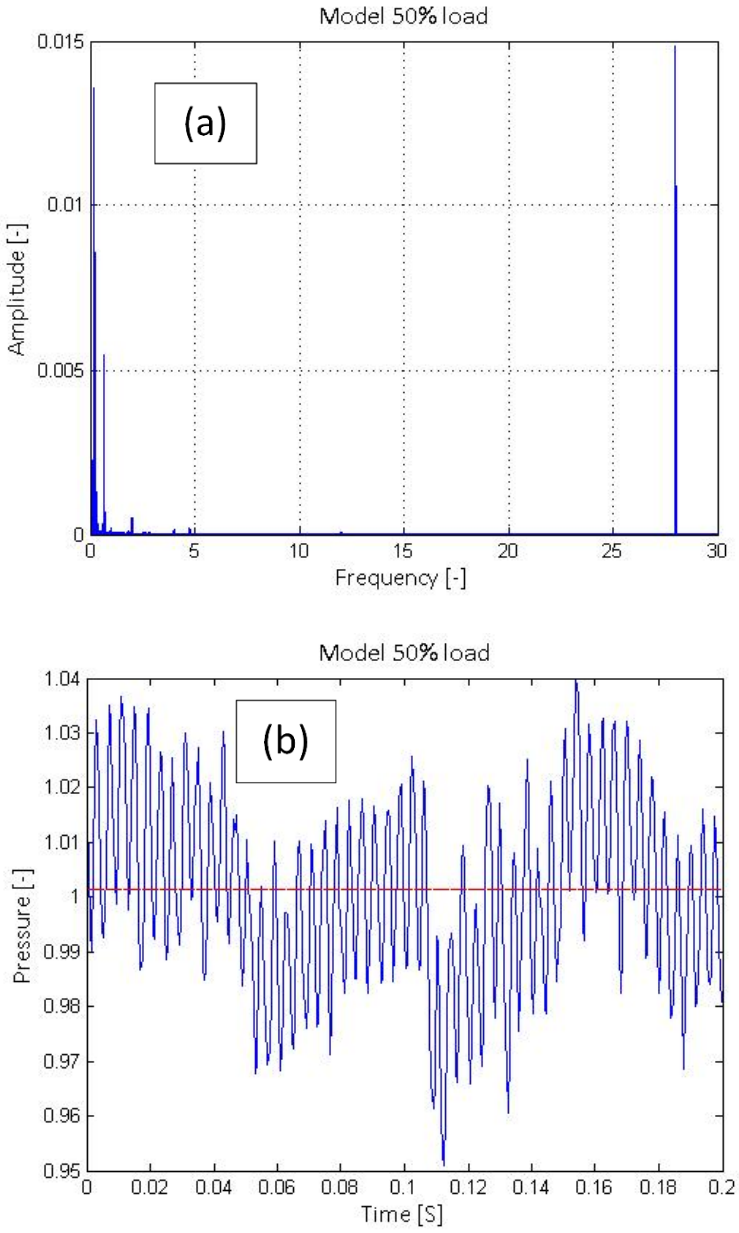

Figure 4.5: Frequency (a) and time (b) domain plot for runner blade transducer on pressure side (Figure 4.2)

The frequency plot form the runner blade transducer showed the guide vane passing frequency as the dominating frequency. It was also evident that the low frequency draft tube vortex was present. Due to the air entering in the draft tube cone this frequency proved to show poor results (Figure 4.4 (a)), the amplitude used to compare with prototype was thus the amplitude to the guide vane passing frequency.

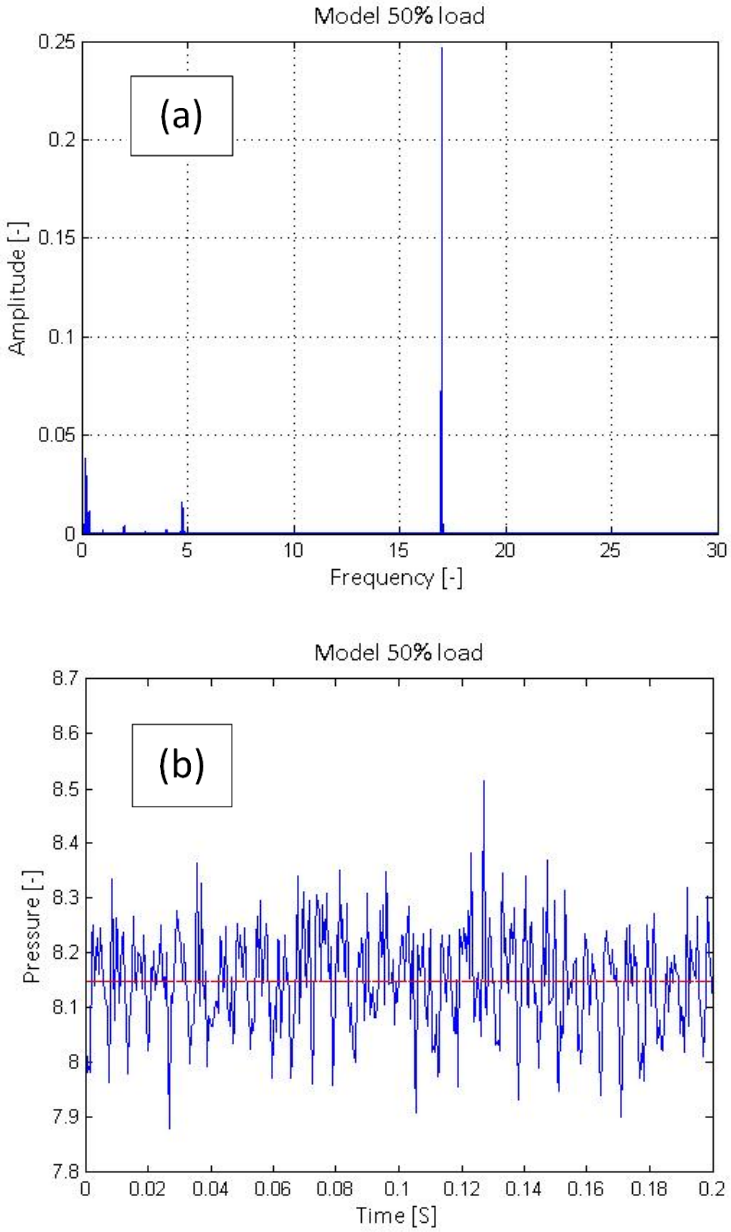

Figure 4.6: Frequency (a) and time (b) domain plot for model vaneless space (Figure 3.2)

For the measurements in the vaneless space, Figure 4.6 (a) showed the runner blade passing frequency as the dominating pressure pulsation frequency. The draft tube vortex frequency was also present, but relatively lower than in the runner. For comparison with prototype the amplitude to the runner blade passing frequency has been regarded.

4.3 Prototype results

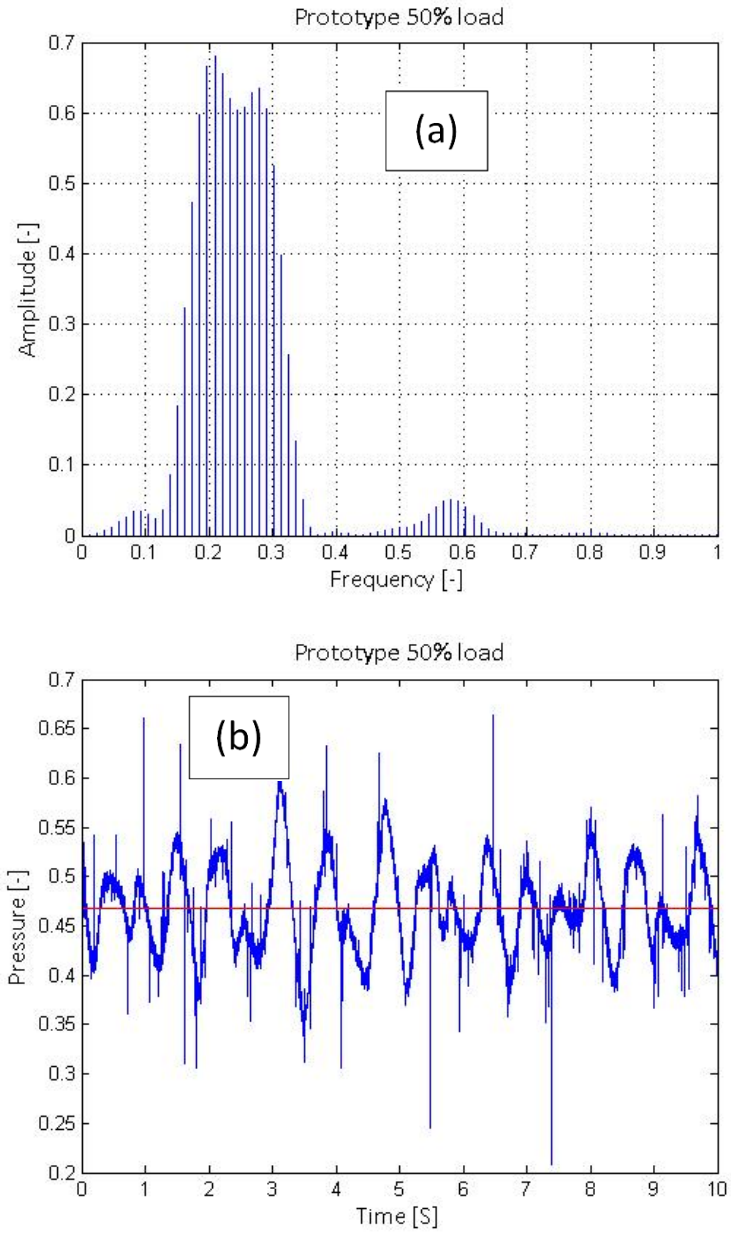

Figure 4.7: Frequency (a) and time (b) domain plot for prototype draft tube

Considering the pressure pulsations in the draft tube the dominating frequency was the draft tube vortex. From analytical calculation the normalized expected frequency was 0.2778. With the estimated deviation of ±20% the interval resulted in 0.2222 to 0.3334. Figure 4.7 showed this frequency interval and the 1st harmonic of the signal in 0.556.

In the time domain plot (Figure 4.7 (b)) there were several drops on the curve. This was most likely to be noise from the transducer. The amplitude estimated for comparison with the model neglected these drops.

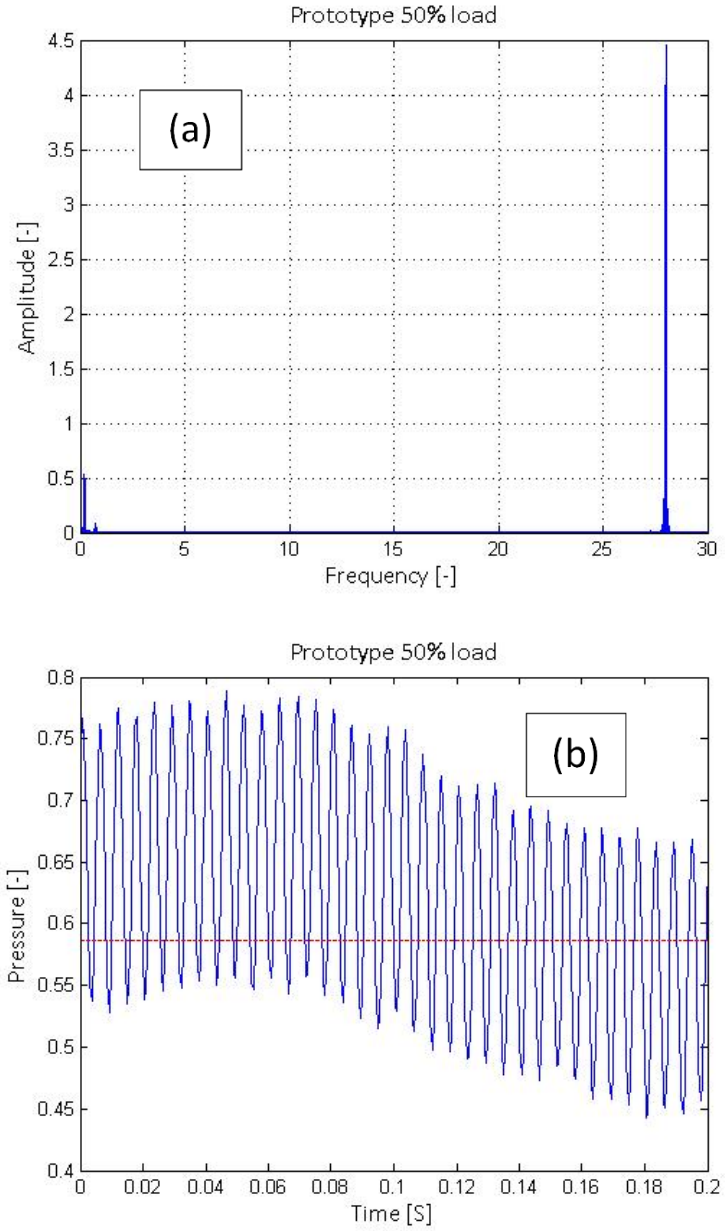

Figure 4.8: Frequency (a) and time (b) domain plot for prototype runner

Measurements from the prototype runner showed the guide vane passing as the dominating frequency (Figure 4.8 (a)). The low frequency draft tube vortex is also present, but due to poor results for the draft tube vortex in the model measurements, the amplitude estimated for comparison with model was only the amplitude of the guide vane passing frequency.

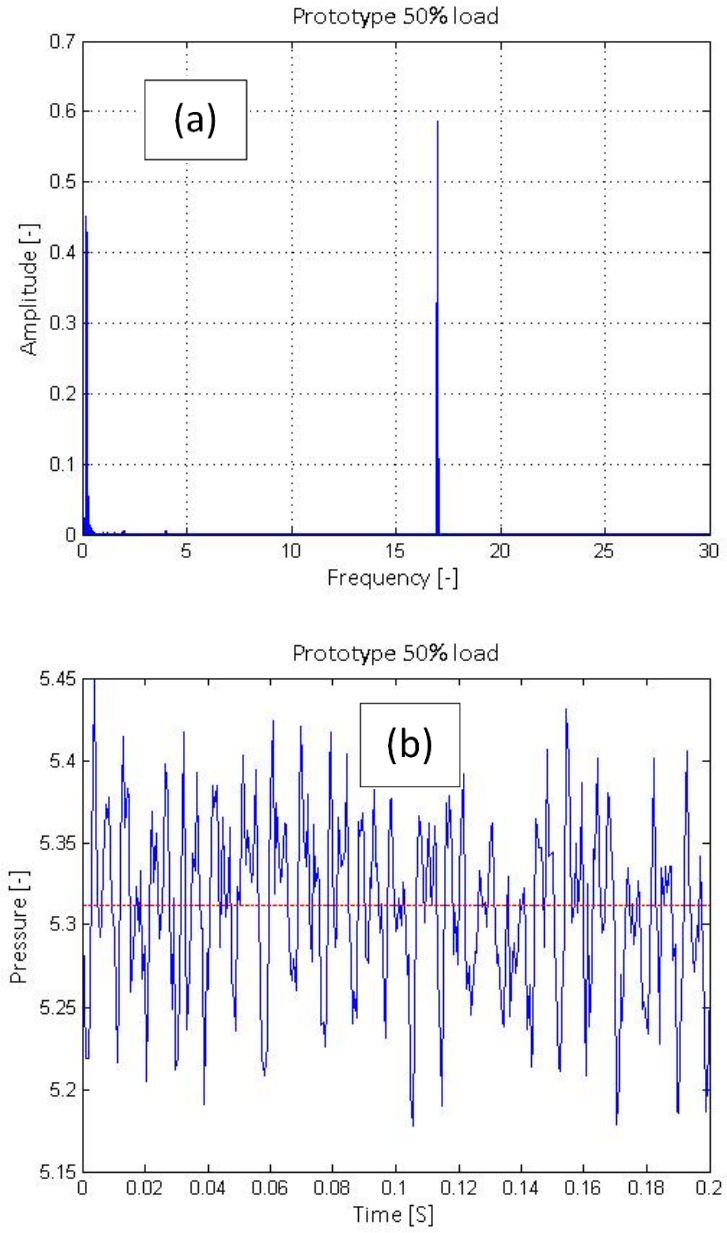

Figure 4.9: Frequency (a) and time (b) domain plot for prototype vaneless space

In the vaneless space both runner blade passing frequency and draft tube vortex frequency were present (Figure 4.9 (a)). For comparison with model the amplitude from the blade passing frequency has been used.

4.4 Comparison between model and prototype

The base for the comparison of the amplitude to the model and the prototype has been founded in section 4.2 and 4.3. In Table 4.2 sampling details for the respective measurements have been summarized. For comparing the amplitudes of the pressure pulsation in the model and prototype turbine, amplitudes have been divided by the reference head. The results have been presented in a scatter plot and a line plot. In the scatter plots, the upper part represents the intensity of the pulsation at different loads. The lower subplot demonstrates the deviation from the suggested scale-up relation in Equation 2.15. One should note that the lower subplot has a lower zoom factor than the upper subplot.

Table 4.2: Logging details for model and prototype

	Logging frequency [Hz]	**Sampling time [s]**
Model Rotating	2000	120
Model Stationary	2000	120
Prototype Rotating	1613	13.8
Prototype stationary	1613	25

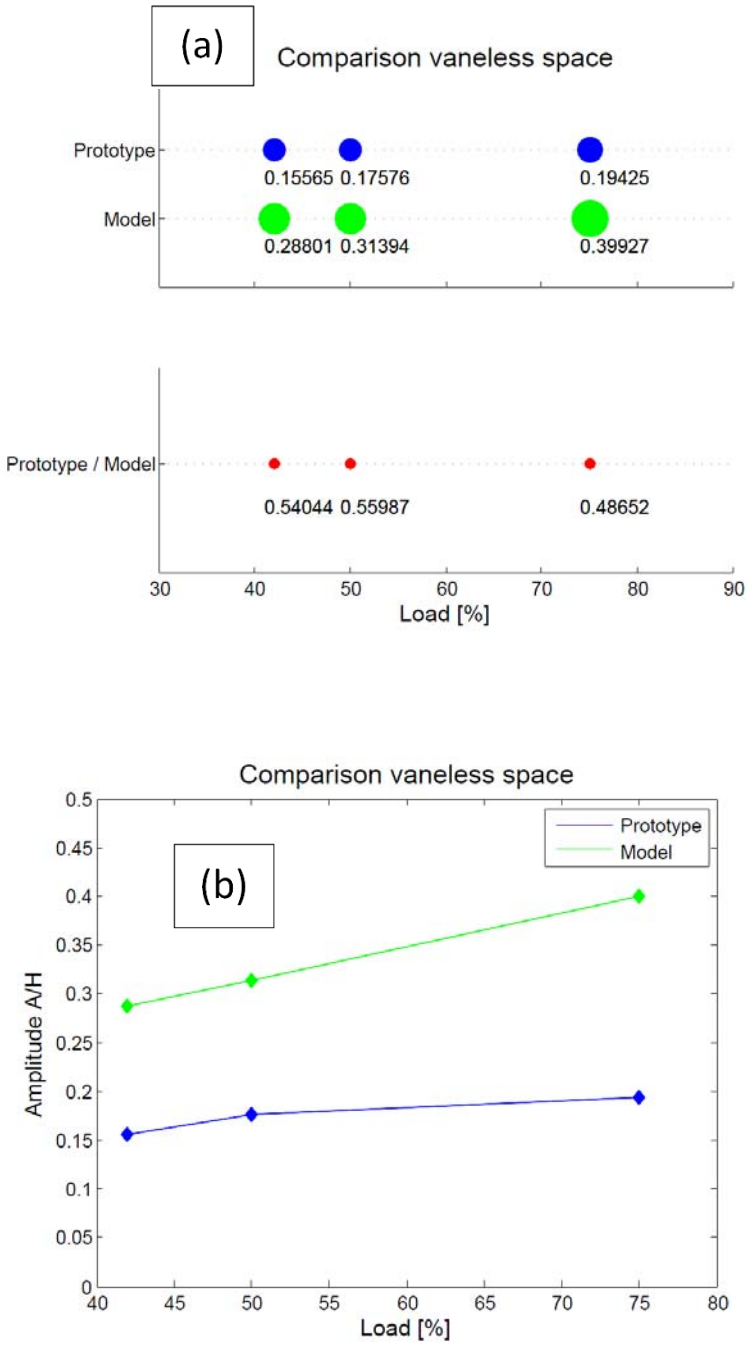

Figure 4.10: Comparison of pressure pulsation amplitudes in the vaneless space

The deviation of the A/H relation in the vaneless space appeared to have linear tendency at low load (Figure 4.10 (a)). At high load it seemed to be an increase in the deviation.

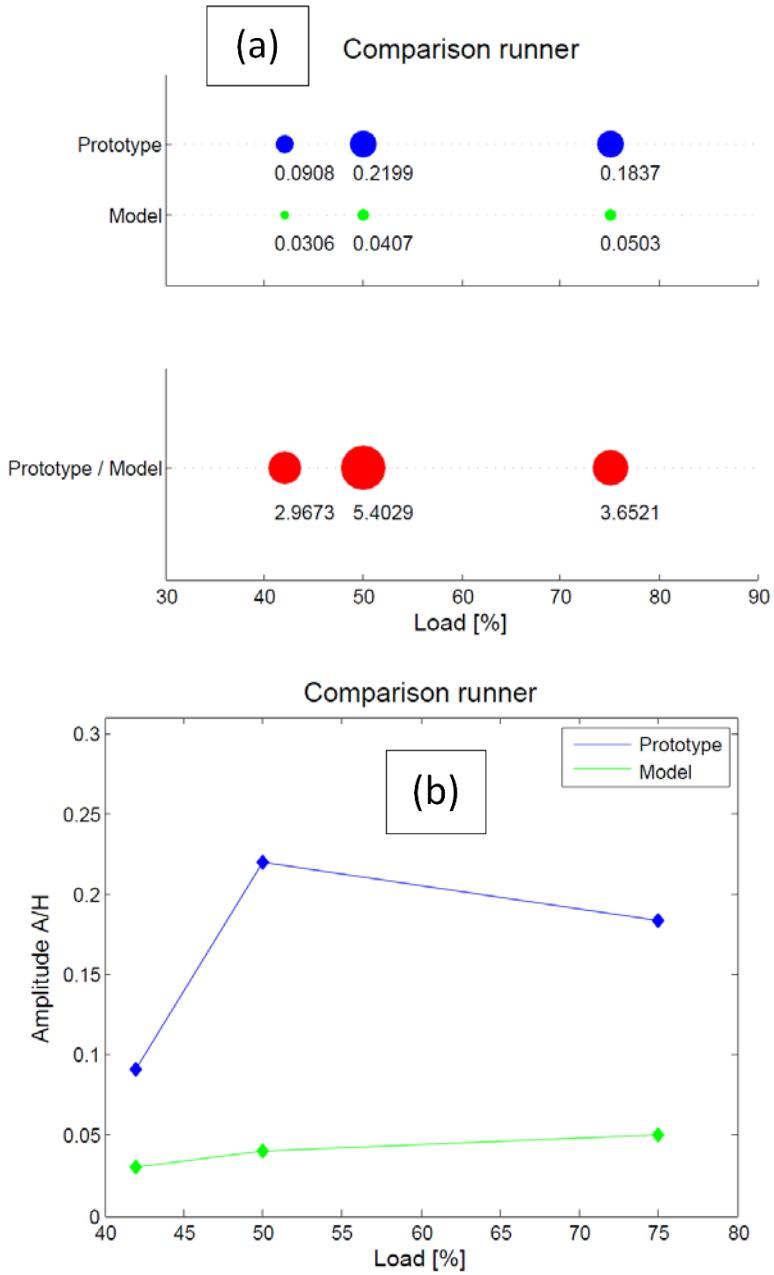

Figure 4.11: Comparison of pressure pulsation amplitudes in the runner

For the A/H relation in the runner, Figure 4.11 (b) indicated a random deviation. At 50 % load the relative amplitude was almost doubled from 42 % load. While it decreased from 50 % to 75 % load.

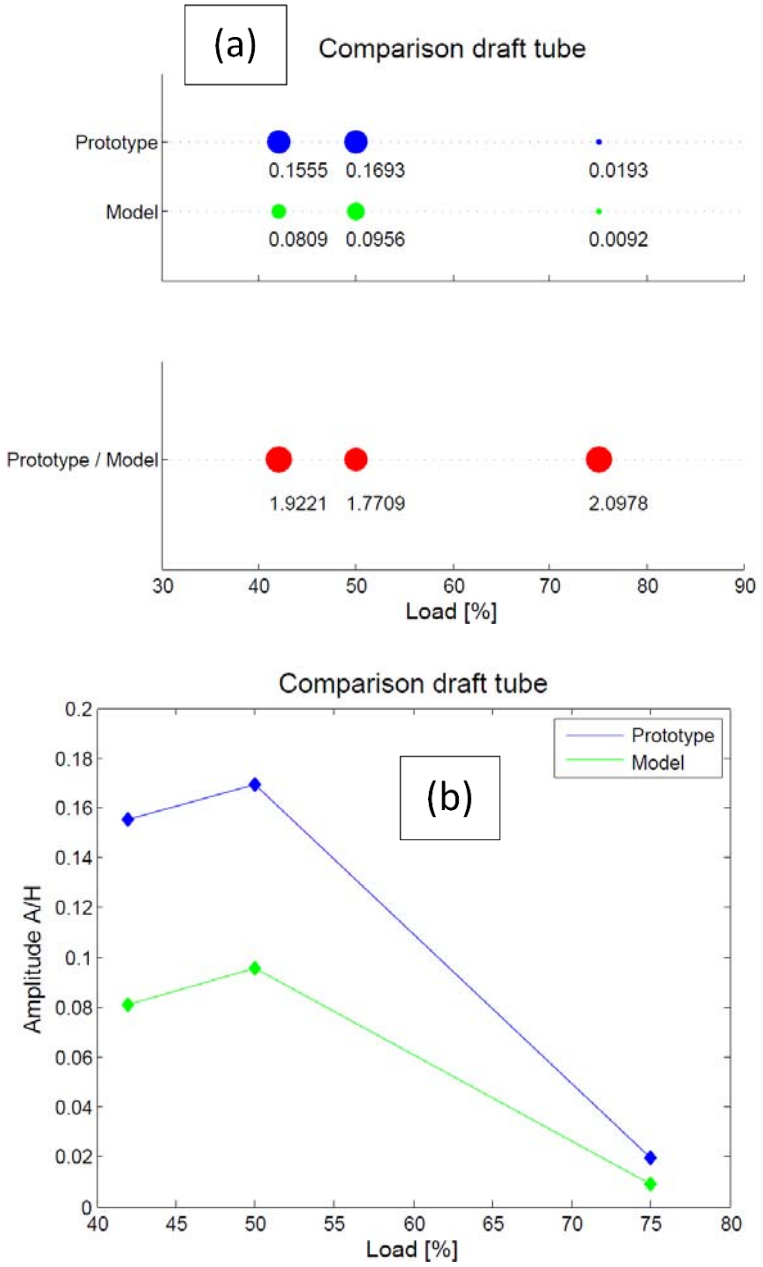

Figure 4.12: Comparison of pressure pulsation amplitudes in the draft tube

The tendencies of the development of the relative amplitudes in the draft tube cone were the same in model and prototype. Considering the result presented for the model turbine (Figure 4.4) the validity of the result can be questioned. It should be taken into account that the amplitude estimated from the model was not calculated at the same relative frequency as in the prototype.

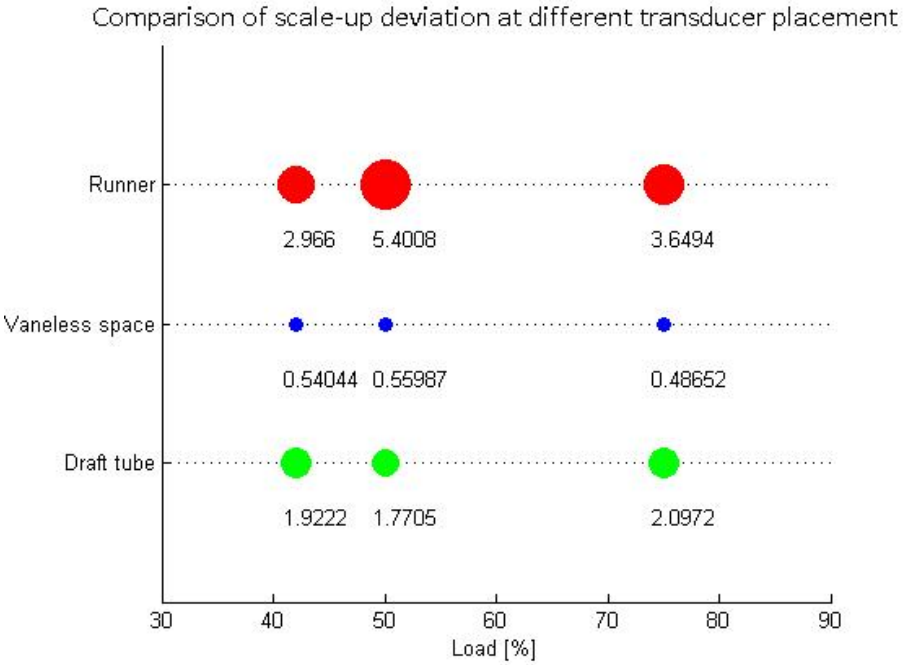

Figure 4.13: Comparison of the deviation of the A/H relation for various transducers at three different loads

To identify if there were a relation between the deviations for the three transducers presented in the result, the deviation were plotted in the same graph (Figure 4.13). The correlation did not indicate any common tendency. The range of deviation was largest for the runner measurements, while in the vaneless space the deviation tended to be constant. For the draft tube cone same tendency was registered, but it must be taken into account that the results from the model turbine might be faulty.

An interesting observation was the high amplitude for the measurements from the vaneless space in the model. This was the only location where the amplitude was relatively higher than the prototype amplitude. This was in contradiction to the result from Audun Tovslid's investigation where the largest amplitudes were found in the prototype for all measurements [3].

4.5 Sigma variation

There has not been conducted sigma variation measurement on the prototype turbine. Thus this section has only been based on data collected from the model tests, and no comparison between model and prototype has been carried out.

Sigma variation was performed at 50 % load with four different values of sigma. Figure 4.14 showed the A/H relation of the pressure pulsation amplitudes. The values in the vaneless space and the runner maintained nearly constant, while in the draft tube the influence from the sigma variation was larger. The amplitude in the draft tube decreased as the sigma level increased, expect at the lowest sigma level where the amplitude was lower than the second lowest sigma level.

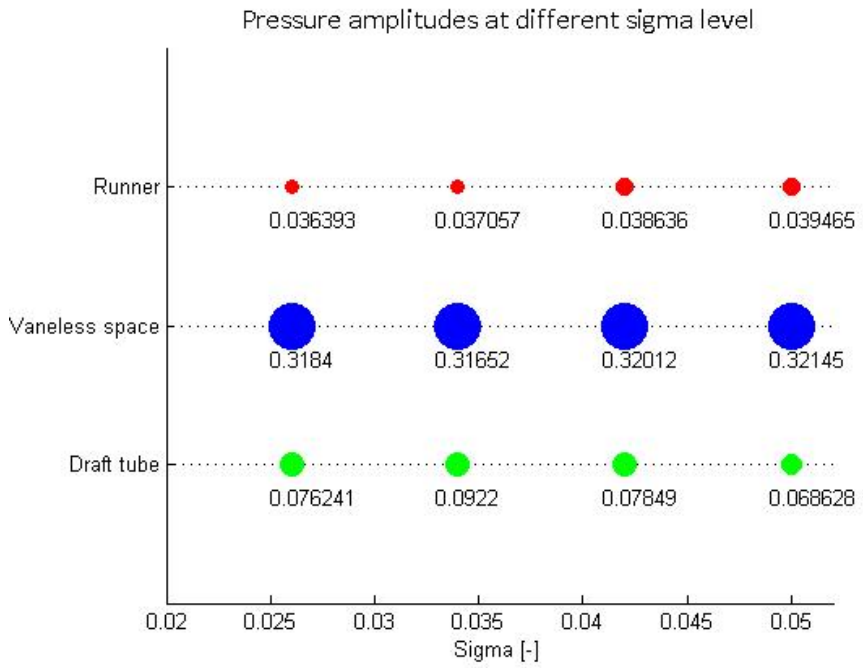

Figure 4.14: Pressure amplitudes at different sigma levels

5 Discussion

5.1 Suggested scale-up relation and deviation from the dimensionless parameters

The aim of this Master's Thesis was to establish a scale-up relation for pressure pulsation in high head Francis turbine. As an attempt the suggested dimensionless parameter A/H has been evaluated. From the theory (chapter 2.3.1) the A/H relation claims to be a function of $\frac{D_1}{D_2}, Q_{ED}, Eu, Ma, n_{ED}, \mathrm{Re}$.

$\frac{D_1}{D_2}$ is defined by the geometrical dimension of the runner and is not adjustable. The model runner was designed to have the same relation as the prototype runner. Q_{ED} and n_{ED} were set in the model test to correspond with the prototype specifications. Thus these fractions have been equal.

As discussed in chapter 3.1.3 the Reynolds number is higher in prototype than model. Thus the model is considered as the limitation. From the logging computer in the laboratory the Reynolds number calculated is in the range of $3.8 \cdot 10^6$ which is 10 % lower than the IEC demand of $4 \cdot 10^6$.

Regarding the deviation between the Mach number and Euler number, graphs made by Audun Tovslid [3] have been used to highlight the problem. The approximate area where measurements have been conducted has been marked with a red square.

The Mach number is based on the speed of sound in water. This has not been measured in either in model nor prototype turbine. The graph (Figure 5.1) has been based on a constant speed of sound of 1200 ms^{-1}, and indicated an increasing deviation of the Mach number between the model and prototype at increasing volume flow.

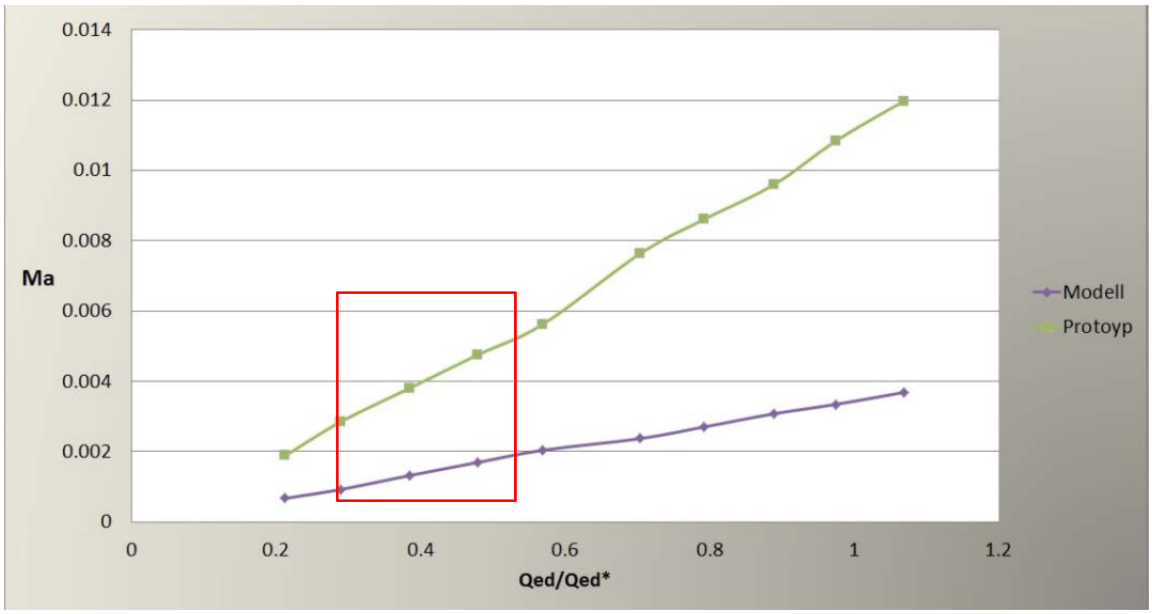

Figure 5.1: Development of Mach number for model and prototype at different loads **[3]**

The Euler number deviation has been presented with the cavitation number (Ka). The cavitation number regards the pressure difference between the vapor pressure and the local pressure. From Figure 5.2 it was evident that the deviation between the model and prototype decreases at high loads, while at low loads the deviation was large. For the measurements conducted at lowest load, the cavitation number deviation was 5 times larger than measurement at the highest load regarded.

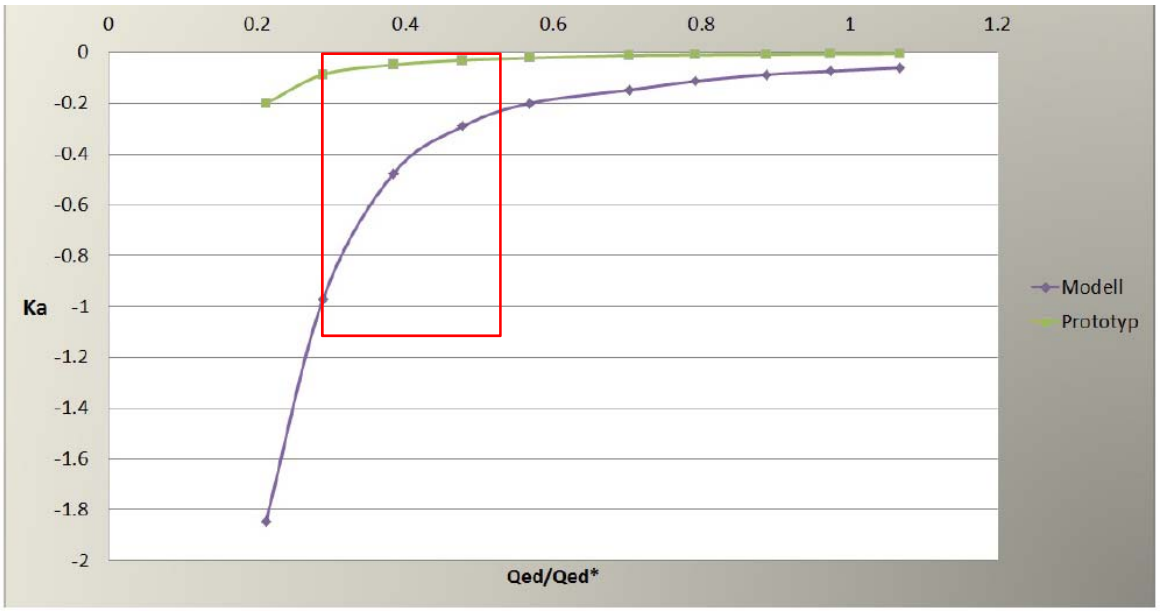

Figure 5.2: Development of Cavitation number (Ka) for model and prototype at different loads **[3]**

5.2 Limitations

Since only three corresponding operation points were used to compare model and prototype, it was not possible to see a trend in the deviation of the scale-up relation. To identify a correlation between the deviation of the Reynolds, Mach and cavitation number it is crucial to have a wide range of operation points.

Moreover the draft tube cone measurements gave results that differed from the expected. This was most likely due to the air sucked into the system. This resulted in comparison of different relative frequencies in the model and the prototype and was most likely to be a source for deviation. The transducers used in the draft tube in the model, were the only dynamic transducers used in the setup.

5.3 Sigma variation

From the theory chapter 2.3 it is expected an increase of the pressure pulsation amplitude when decreasing the sigma level. From Figure 4.14 the result showed the same trend with exception of the lowest sigma level. There might be several reasons for this. Firstly it can be due to the air entering in the draft tube cone. Secondly there was a leakage in the draft tube tank where the vacuum pump regulated the pressure and hence the sigma level. It was not obtainable to maintain the pressure constant thus the sigma level increased with time. Especially at very low sigma levels, it was challenging to maintain the pressure.

6 Conclusion

The suggested A/H relation as a pressure pulsation amplitude scale-up did not prove to give any indication of being correct. In the vaneless space the tendency of increase in the amplitude in both model and prototype were similar, however a factor needs to be added to the scale-up relation.

There were several dissimilarities between the model and prototype test conditions and these were most likely to be the source for the deviation. Especially attention should be drawn to the Mach number where the deviation increases when the load increases. Moreover the cavitation number deviation proved to be significant at low loads.

Regarding the sigma variation influence the results showed largest influence in the draft tube, minor influence in the runner and close to no influence in the vaneless space. However the results were not to be trusted due to the air entering in the draft tube, so no actual conclusion could be drawn. Nevertheless the trend of an increase of the amplitude at decreasing the sigma level is reasonable.

7 Further work

To continue the investigation of scale-up relation for high head Francis turbine, more measurement of the model turbine considered in this Master's Thesis should be conducted. The data acquisition system proved be well functioning, but improvement on the rotating logging system could be implemented. The cRIO installed on the shaft has a limited memory and can only save eight logging points with the sampling rate of 2000 Hz for 120 second. This means the rig has to be stopped to empty the memory. To make the system more convenient a wireless router can be installed to transfer data on demand. Other possibilities is to use a memory card module and write data from the cRIO memory to the memory card installed, or transfer data through a slip ring. It is important to keep in mind that data transferring cannot be done when the cRIO is logging since this can cause disturbance in the logging.

From the prototype measurements there exist pressure pulsation data for 14 operation point. If all the corresponding operation point were to be conducted for the model turbine, a better base for comparison would be founded. Moreover the pressure transducer which failed on the runner blade should be replaced. This will enable comparison of the data from all the transducers in the prototype.

For further work on the model turbine it is crucial with improvements to prevent air suction into the draft tube cone. Considering the cavitation influence on sigma variation it is essential that air is not sucked into the drat tube cone for obtaining good results.

When it comes to equipment used in the setup, verification of the dynamic transducers in the draft tube cone should be considered. Calibration reports on two of these transducers were lacking and they should be recalibrated with adequate equipment.

8 References

[1] E. Kobro, "Measurement of Pressure Pulsations in Francis Turbines," Norwegian University of Science and Technology, Trondheim, 2010.

[2] W. J. Rheingans, "Power Swings in Hydroelectric Power Plants," Milwaukee, 1940.

[3] A. Tovslid, "Trykkpulasjoner i Francisturbiner - sammenligning av modell og prototypmålinger," NTNU, Trondheim, 2012.

[4] T. Nielsen, "Lecture note: Model test," 2012.

[5] J. Haugen, "Laboratoriet - Typiske frekvenseri strømningsmaskiner," 1994.

[6] T. Nielsen, "Dynamisk dimensjonering av vannkraftverk," Trondheim, 1990.

[7] H. Brekke, Pumper & Turbiner, Trondheim: Vannkraftlaboratoriet, 2003.

[8] F. M. White, Fluid Mechanics, New York: McGraw Education, 2008.

[9] T. Nielsen, Lecture note: Dimensional analysis, 2012.

[10] IEC, "Hydraulic machines, radial and axial - Performance conversion method from model to prototype," The International Electrotechnical commission, Geneva, Switzerland, 2009.

[11] A. L. Wheeler and A. R. Ganji, Introduction to Engineering Experimentation, Upper Saddle River, New Jersey: Pearson Education, 2004.

[12] G. Heinzel, R. A. and R. Schilling, "Spectrum and spectral density estimation bythe Descrete Fourier transform (DFT), including a comprehensive list of window fubctions and some new flat-top windows," Teilinstitut Hannover, Hannover, 2002.

[13] P. Doerfler, "Memorandum from Andritz," 2012.

[14] P. P. Jonsson, "Flow and Pressure Measurements in Low-Head Hydraulic Turbines," Luleå University of Technology, Luleå, 2011.

[15] A. M. Tørklep, "Pressure oscillations during start and stop of a high head Francis turbine," NTNU, Trondheim, 2012.

[16] "National Instuments," National Instuments, [Online]. Available: http://www.ni.com/white-paper/6983/en. [Accessed 13 05 2013].

A Calibration reports

Calibration report for runner transducer

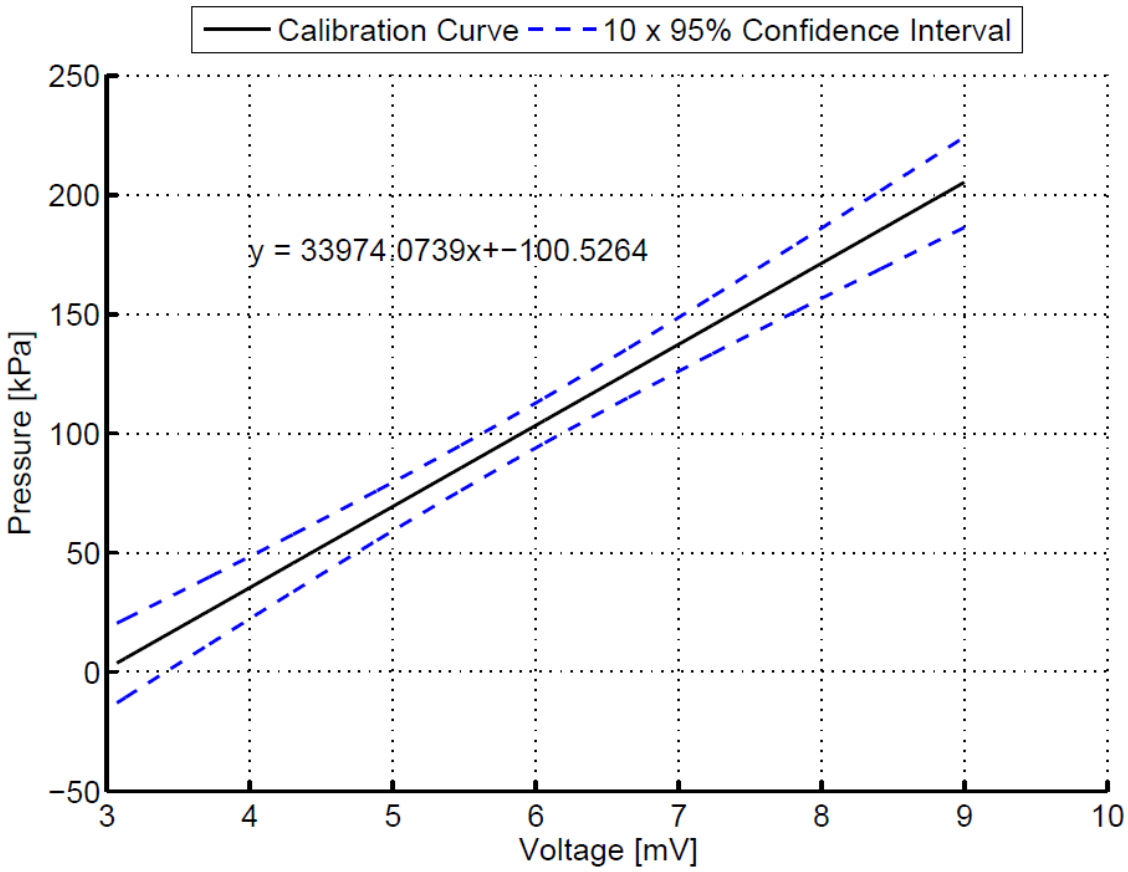

Calibration report for inlet transducers

CALIBRATION REPORT

CALIBRATION PROPERTIES
Calibrated by: Julie Marie Hovland og Ingeborg Lassen Bue
Type/Producer: Druck PTX 1400
SN: Y21674\07
Range: 0-10 bar g
Unit: kPa

CALIBRATION SOURCE PROPERTIES
Type/Producer: Pressurements deadweight tester P3223-1
SN: 66256
Uncertainty [%]: 0,01

POLY FIT EQUATION:
Y= -148.91611524E+0X^0 + 125.07688471E+0X^1

CALIBRATION SUMARY:
Max Uncertainty : 0.269190 [%]
Max Uncertainty : 0.268971 [kPa]
RSQ : 0.999998
Calibration points : 12

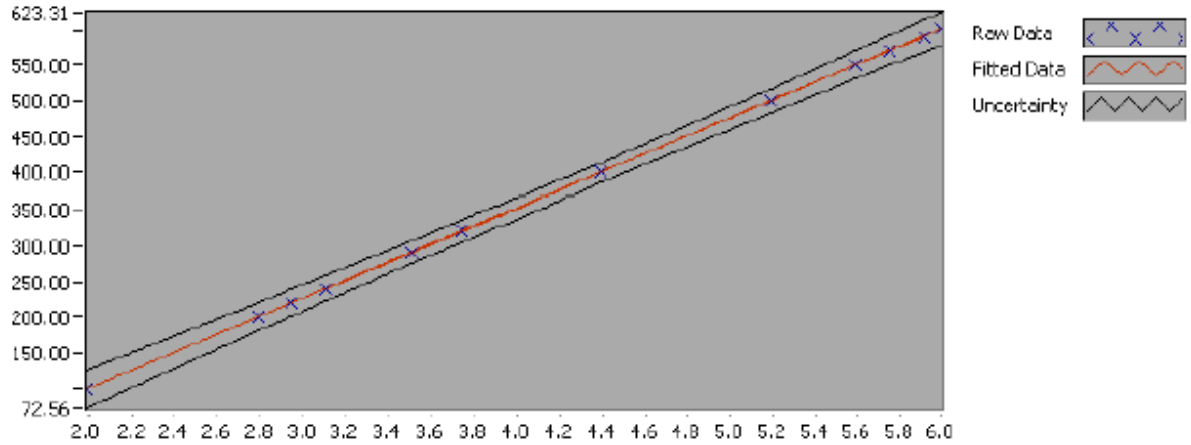

Figure 1 : Calibration chart (The uncertainty band is multiplied by 100)

CALIBRATION REPORT

CALIBRATION PROPERTIES
Calibrated by: Julie Marie Hovland og Ingeborg Lassen Bue
Type/Producer: Druck PTX 1400
SN: Y21674\07
Range: 0-10 bar g
Unit: kPa

CALIBRATION SOURCE PROPERTIES
Type/Producer: Pressurements deadweight tester P3223-1
SN: 66256
Uncertainty [%]: 0,01

POLY FIT EQUATION:
Y= -147.56618266E+0X^0 + 124.99731727E+0X^1

CALIBRATION SUMARY:
Max Uncertainty : 0.067709 [%]
Max Uncertainty : 0.124951 [kPa]
RSQ : 1.000000
Calibration points : 12

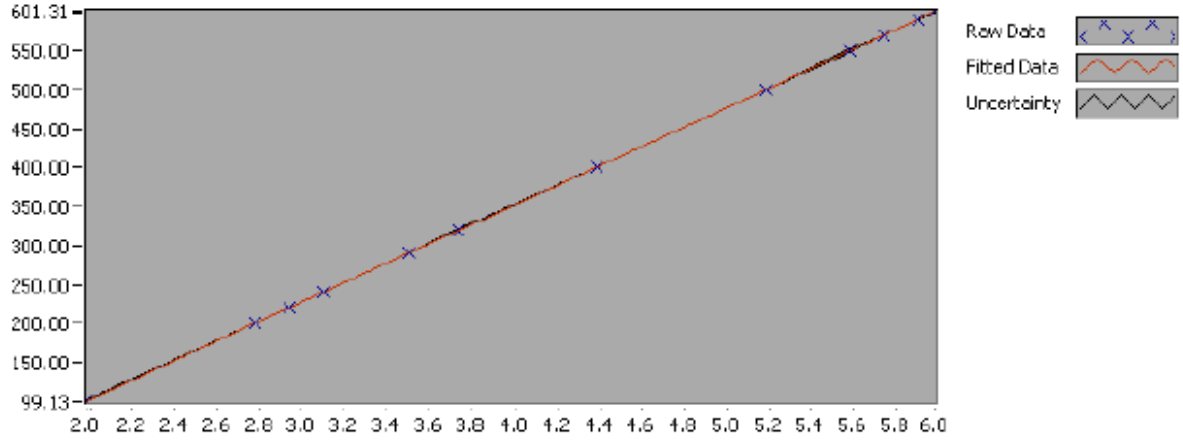

Figure 1 : Calibration chart (The uncertainty band is multiplied by 10)

Calibration report for draft tube transducer

CALIBRATION REPORT

CALIBRATION PROPERTIES
Calibrated by: Julie Marie Hovland and Ingeborg Lassen Bue
Type/Producer: Druck PTX 610
SN: 3811122
Range: 0-2,5 bar a
Unit: kPa

CALIBRATION SOURCE PROPERTIES
Type/Producer: Pressurements deadweight tester P3223-1
SN: 66256
Uncertainty [%]: 0,01

POLY FIT EQUATION:
Y= + 96,49286232E+0X^0 + 312,33999201E-3X^1

CALIBRATION SUMARY:
Max Uncertainty : 0,010627 [%]
Max Uncertainty : 0,010379 [kPa]
RSQ : 1,000000
Calibration points : 27

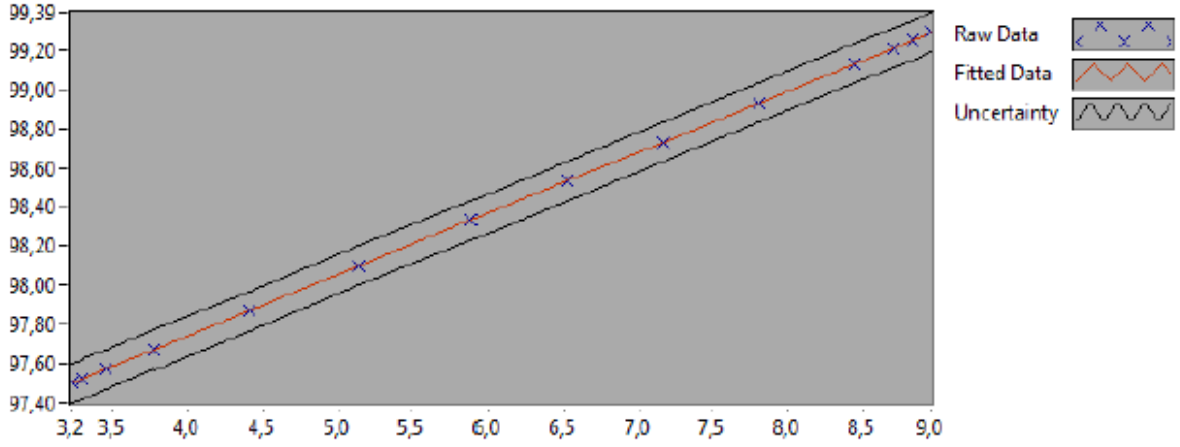

Figure 1 : Calibration chart (The uncertainty band is multiplied by 10)

Calibration report for vaneless space transducers

CALIBRATION REPORT

CALIBRATION PROPERTIES
Calibrated by: Julie Marie Hovland, Ingeborg Lassen Bue
Type/Producer: Kulite XTE-190
SN: v4537-23
Range: 0-3.5 bar a
Unit: kPa

CALIBRATION SOURCE PROPERTIES
Type/Producer: Pressurements deadweight tester P3223-1
SN: 66256
Uncertainty [%]: 0,01

POLY FIT EQUATION:
Y= + 13.46620876E+0X^0 + 70.31068838E+3X^1

CALIBRATION SUMARY:
Max Uncertainty : 0.026225 [%]
Max Uncertainty : 0.026147 [kPa]
RSQ : 1.000000
Calibration points : 19

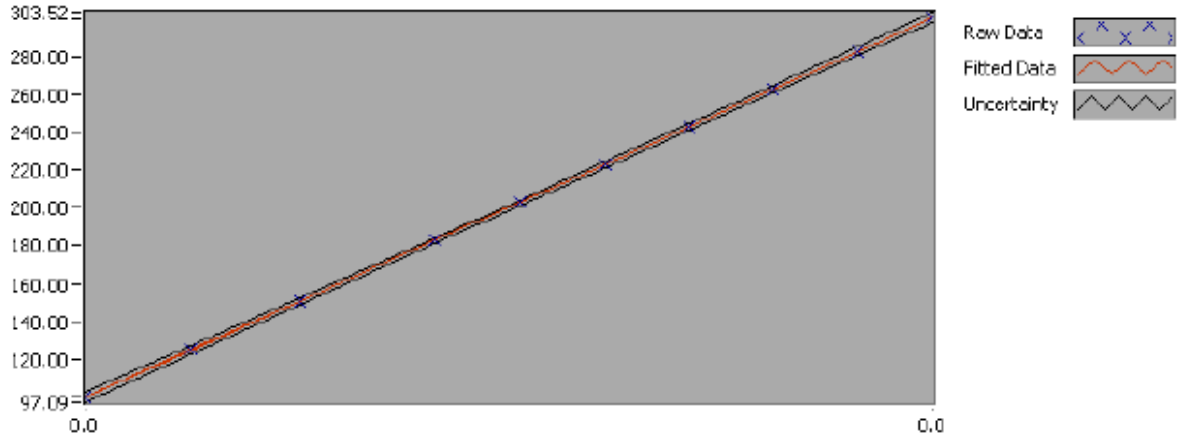

Figure 1 : Calibration chart (The uncertainty band is multiplied by 100)

CALIBRATION REPORT

CALIBRATION PROPERTIES
Calibrated by: Julie Marie Hovland, Ingeborg Lassen Bue
Type/Producer: Kulite XTE-190
SN: v4537-33
Range: 0-7 bar a
Unit: kPa

CALIBRATION SOURCE PROPERTIES
Type/Producer: Pressurements deadweight tester P3223-1
SN: 66256
Uncertainty [%]: 0,01

POLY FIT EQUATION:
Y= + 54.48242625E+0X^0 + 154.91703928E+3X^1

CALIBRATION SUMARY:
Max Uncertainty : 0.073561 [%]
Max Uncertainty : 0.073340 [kPa]
RSQ : 0.999998
Calibration points : 20

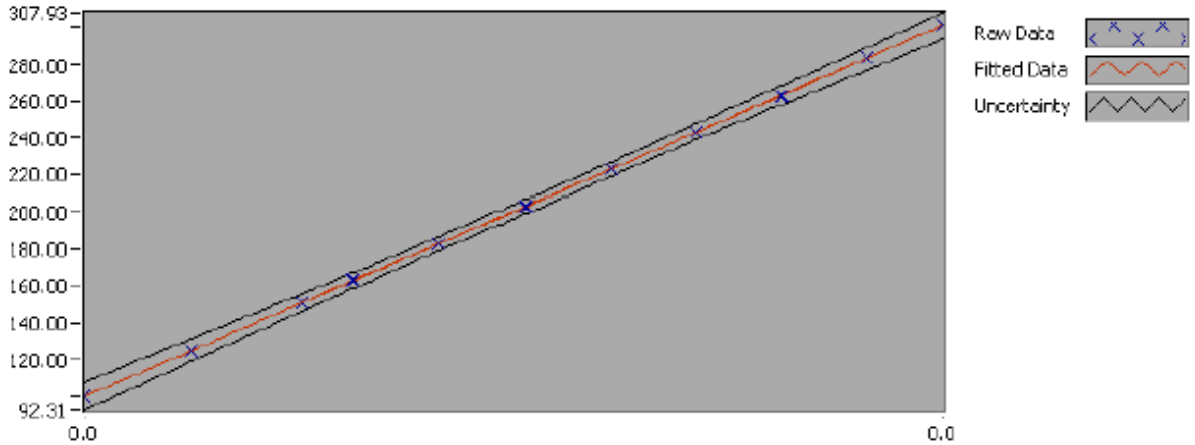

Figure 1 : Calibration chart (The uncertainty band is multiplied by 100)

CALIBRATION REPORT

CALIBRATION PROPERTIES
Calibrated by: Julie Marie Hovland, Ingeborg Lassen Bue
Type/Producer: Kulite XTE-190
SN: v4537-33
Range: 0-7 bar a
Unit: kPa

CALIBRATION SOURCE PROPERTIES
Type/Producer: Pressurements deadweight tester P3223-1
SN: 66256
Uncertainty [%]: 0,01

POLY FIT EQUATION:
Y= + 99.64090291E+0X^0 + 140.82223184E+3X^1

CALIBRATION SUMARY:
Max Uncertainty : 0.110693 [%]
Max Uncertainty : 0.110582 [kPa]
RSQ : 0.999998
Calibration points : 21

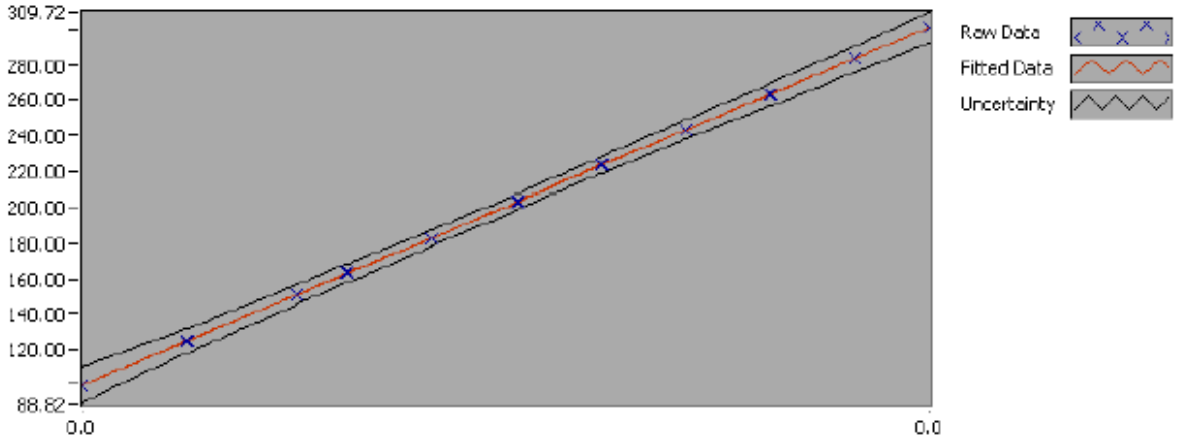

Figure 1 : Calibration chart (The uncertainty band is multiplied by 100)

Calibration report for draft tube cone transducer

RAINPOWER

CALIBRATION REPORT

Parameter:	Pressure pulsations / dynamic pressure
Object identity:	Transducer VKL1740580 + amplifier VKL5015/1719297

Calibration equipment and settings:

Amplifier:	VKL5015: 81.1pC/bar, 0.1bar/V, no filter, "Medium" mode ("Long" for calibration)
Oscilloscope:	MR 8001: DC, 20ms/div, 0.5 -2V/div, trig level 1-0.3V, single seq. trig, noise rej.
DVM:	MD 1007: DCV, resolution x.xxV, speed 3
Pressure reference:	ME 110

Calibrated range:
100 kPa

Reference pressure [kPa]	Output [V]	Lin. est. [kPa]	Deviation [kPa]	[%] OR
97.1	9.62	97.2	0.1	0.1
64.0	6.31	63.8	-0.2	-0.2
42.0	4.18	42.2	0.2	0.2
27.8	2.74	27.7	-0.1	-0.1
18.5	1.83	18.5	0.0	0.0

Calibration constants:

C_1[kPa/V]	C_0[kPa] 1)
10.10	**0.0**

1) C0=0 in the data acq. program

Date / sign.: 2010-11-17

VKL0580_pp402_2010-11-17.xlsx

Calibration report for torque

CALIBRATION REPORT

CALIBRATION PROPERTIES
Calibrated by: Julie Marie Hovland og Ingeborg Lassen Bue
Type/Producer: Kraftcelle
SN:
Range:
Unit: Nm

CALIBRATION SOURCE PROPERTIES
Type/Producer: HBM 500kg load cell
SN: V4536-4
Uncertainty [%]: 0.01

POLY FIT EQUATION:
Y= -197.79087116E+0X^0 + 488.34575988E+0X^1

CALIBRATION SUMARY:
Max Uncertainty : Inf [%]
Max Uncertainty : 1.299025 [Nm]
RSQ : 0.999990
Calibration points : 30

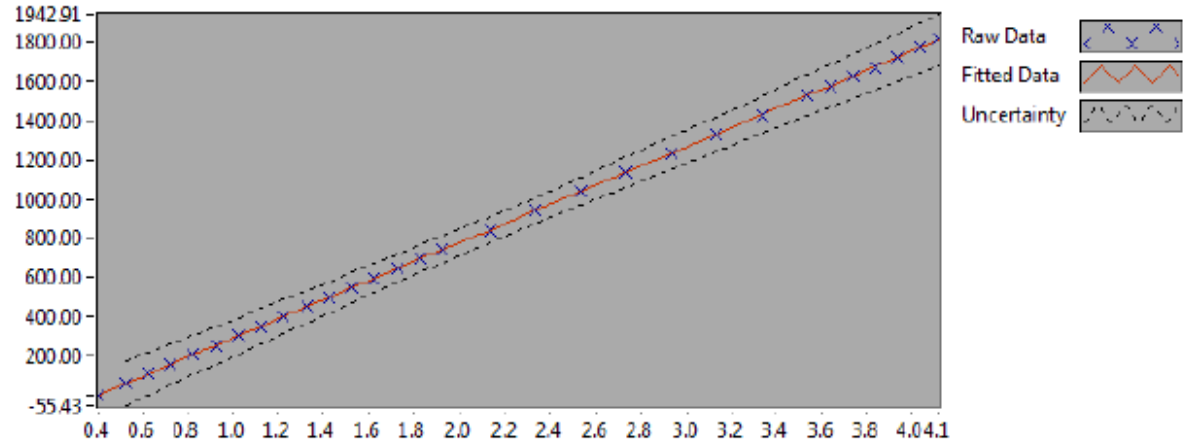

Figure 1 : Calibration chart (The uncertainty band is multiplied by 100)

```
%% Calibration of raw data

clearvars -except cal

ind_samples=1;

mappe= uigetdir;
filepattern=strcat(mappe,'\*.xlsx');
% filepattern=fullfile('M:','MATLAB','Resultat','*.xlsx');
xlsxfiles=dir(filepattern);
length=(length(xlsxfiles))/(2*ind_samples)-2;   %Number of samples (divided by two since
results from the RIOs are saved in separate files.

nsamples=29999;
ncolumns1=12;
ncolumns2=11;
p=104.816152;

%% Calibration stasjonære målinger

for k=1:length
    for h=1:ind_samples
        data{k,h}(:,1)= cal{k,h}(:,1)*10.1;
        data{k,h}(:,2)= cal{k,h}(:,2)*10;
        data{k,h}(:,3)= cal{k,h}(:,3)*10;
        data{k,h}(:,4)= (cal{k,h}(:,4)*488.34575988)-197.79087116;
        data{k,h}(:,5)= (cal{k,h}(:,5)*124.99731727)-147.56618266;
        data{k,h}(:,6)= (cal{k,h}(:,6)*125.07688471)-148.91611524;
        data{k,h}(:,7)= (cal{k,h}(:,7)*(31.247519))-62.4527;

        for j=1:nsamples
            if cal{k,h}(j,8) <= 1
                data{k,h}(j,8)= 0;
            else
                data{k,h}(j,8)= 1;
            end
        end



            data{k,h}(:,9)= (cal{k,h}(:,9).*(-70.31068838*1000))+13.46620876;
            data{k,h}(:,10)= (cal{k,h}(:,10).*(-154.91703928*1000))+54.48242625;
            data{k,h}(:,11)= (cal{k,h}(:,11).*(-140.82223184*1000))+99.64090291;
            data{k,h}(:,12)= (cal{k,h}(:,12)).*1e-6;


  %% Calibration roterende målinger

            for j=1:nsamples
                if cal{k,h+ind_samples}(j,1) <= 1
                    data{k,h+ind_samples}(j,1)= 0;
                else
                    data{k,h+ind_samples}(j,1)= 1;
                end
            end
```

```
            data{k,h+ind_samples}(:,2)= (cal{k,h+ind_samples}(:,2).*(33974.0739))-100.5264+p;
            data{k,h+ind_samples}(:,3)= (cal{k,h+ind_samples}(:,3).*1e-6);


%             data{k,h+ind_samples}(:,2)= (cal{k,h+ind_samples}(:,2).*(34194.785))-97.5116+p;
%             data{k,h+ind_samples}(:,3)=
(cal{k,h+ind_samples}(:,3).*(34501.0394))-106.5909+p;
%             data{k,h+ind_samples}(:,4)=
(cal{k,h+ind_samples}(:,4).*(34113.1243))-109.4301+p;
%             data{k,h+ind_samples}(:,5)= (cal{k,h+ind_samples}(:,5).*(34388.0562))-97.4117+p;
%             data{k,h+ind_samples}(:,6)=
(cal{k,h+ind_samples}(:,6).*(33974.0739))-100.5264+p;
%             data{k,h+ind_samples}(:,7)=
(cal{k,h+ind_samples}(:,7).*(34292.9657))-101.5059+p;
%             data{k,h+ind_samples}(:,8)= (cal{k,h+ind_samples}(:,8).*(34175.6596))-97.1283+p;
%             data{k,h+ind_samples}(:,9)= (cal{k,h+ind_samples}(:,9).*(34078.753))-108.9612+p;
%             data{k,h+ind_samples}(:,10)=
(cal{k,h+ind_samples}(:,10).*(34180.686))-92.9927+p;
%             data{k,h+ind_samples}(:,11)= (cal{k,h+ind_samples}(:,11).*1e-6);

        end
    end



clearvars -except cal data
save('caldata')
```

```
clear all

% load('ProtoRunnerAmp.mat')
% load('ModelRunnerAmp')
% %
% load('ModelGVAmpl.mat')
% load('ProtoGVAmpl')
%
% load('ModelDTAmpl')
% load('ProtoDTAmpl')

y2=[2 2 2];
y=[1 1 1];

last=[42 50 75];
zoom=1000;
zoomdiff=100;
diff=(ampl./amplM);


figure(1)

subplot(2,1,1)
    scatter(last,y,zoom.*amplM,'filled','g'); hold on;
    scatter(last,y2,zoom.*ampl,'filled','b'); hold on;


set(gca,'YTickLabel', {'Model', 'Prototype'}, 'YTick',[1 2]);
set(gca,'XTickLabel', {});
title('Comparison draft tube','FontSize',14,'FontName','Calibri')
set(gcf,'color','w');
set(gca, 'YGrid', 'on', 'XGrid', 'off')


plottetemp(2,:)=amplM;
plottetemp(3,:)=ampl;

x=[42 50 75];

for j=2:3
    for i=1:3
        k=x(i);
        text(k-1,j-1.4,num2str(plottetemp(j,i)))
    end
end

xlim([30,90]);
ylim([0,3]);


 subplot(2,1,2)
    scatter(last,y,zoomdiff.*diff,'filled','r'); hold on;

    plottetemp(1,:)=diff;

x=[42 50 75];
```

```
for j=1:1
    for i=1:3
        k=x(i);
        text(k-1,j-0.4,num2str(plottetemp(j,i)))
    end
end



xlabel ('Load [%]','FontSize',12,'FontName','Calibri');
%set(gca,'YTickLabel', '$$\frac{1}{2}$$');%,'YTick',[1]);
set(gca,'YTickLabel', 'Prototype / Model', 'YTick',[1]);
%ylabel('$\frac{\mathrm{Prototype}}{Model}$', 'Interpreter', 'latex', 'FontSize', 16, 'rot',
0,'FontName','Calibri');
set(gcf,'color','w');
set(gca, 'YGrid', 'on', 'XGrid', 'off')

xlim([30,90]);
ylim([0,1.9]);




%%

figure(2)

plot(last,ampl,'Color',1/255*[0 255 0]); hold on;
plot(last,amplM,'Color',1/255*[0 0 255]); hold on;
plot(last,ampl,'gd','MarkerFaceColor','g'); hold on;
plot(last,amplM,'bd','MarkerFaceColor','b'); hold on;
set(gcf,'color','w');
xlabel ('Load [%]','FontSize',12,'FontName','Calibri');
ylabel ('Amplitude A/H','FontSize',12,'FontName','Calibri');
legend ('Model','Prototype');
title('Comparison draft tube','FontSize',14,'FontName','Calibri');
xlim([40,80]);
ylim([0,0.25]);

%clearvars -except  amplitudeM pksThrM pksThrminM  amplitude pksThr pksThrmi
```

```
%clearvars

%DTdata=load('Kalibrert_USB_Trykk_16_22_59_26562500.dat');          %velg driftspunkt
%importer filer
clearvars -except ampl
load('RunnerMat.mat') %{42 50 75}

Col=[1 2 3 4 5 6 7];
c=[1 2 3 4 5 6 7];
nsamples=22199;
ncolumns=7;
tr=3;  %velger transduser
OP=2;   %velger driftspunkt 1=42, 2=50, 3=75
HP=377;

for i=1:nsamples
    for k=1:ncolumns
        rmat(i,k)=mat{1,OP}(i,k);            %velge driftspunkt
    end
end
temp2D(1:nsamples,1:7)=rmat(1:nsamples,c);


%% kalibreringsverdier
mat=rmat;
for k=1:nsamples
    temp2D(:,1)=mat(:,1);
    temp2D(:,2)=(mat(:,2).*0.00000104+0.042).*100;
    temp2D(:,3)=(mat(:,3).*0.00000104+0.0373).*100;
    temp2D(:,4)=(mat(:,4).*0.00000104+0.0328).*100;
    temp2D(:,5)=(mat(:,5).*0.00000104+0.0413).*100;
    temp2D(:,6)=(mat(:,6).*0.00000104+0.0352).*100;
    temp2D(:,7)=(mat(:,7).*0.00000104+0.0466).*100;

end

%%
%Normaliserer
for i=1:ncolumns
    temp2D_rms(:,i)=temp2D(:,i)-rms(temp2D(:,i));
end



Fs=1613;
nfft=nsamples;
L=floor(nfft/2+1);


pwelchArray2D=zeros(L,3);
pwelchArray3D=zeros(L,3,ncolumns);
y=zeros(L,1);
T=(0:1:nfft-1)/Fs;

window_weight=(L/2);
overlapPercent=70;
```

```
for i=1:ncolumns
    [pxx,f] = pwelch(temp2D_rms(:,i), hanning(window_weight),overlapPercent, nfft,Fs);


    for j=1:L
     y(j)=Col(:,i);

    end

 pwelchArray2D=[f y pxx];
 pwelchArray3D(:,:,i)=(pwelchArray2D);

end

g=pwelchArray3D(:,1,tr);
h=pwelchArray3D(:,3,tr);

%normaliserer
for i=1:ncolumns
    temp2D(:,i)=temp2D(:,i)./HP;
end

%% plotter
Fig=figure('Color',[1 1 1]);

box('on');hold('all');
dcm_obj = datacursormode(Fig);
%set(dcm_obj,'UpdateFcn',@display_data,'DisplayStyle','datatip','SnapToDataVertex','off','Enab
le','on');
%set(gca,'YTickLabel', {});%,'YTick',[]);
grid on

stem(g/6.25,h/HP,'Marker','none','Color',1/255*[0 0 255]);
xlabel ('Frequency [-]','FontSize',12,'FontName','Calibri');
ylabel ('Amplitude [-]','FontSize',12,'FontName','Calibri');
title('Prototype 50% load','FontSize',14,'FontName','Calibri');
xlim([0,30])


figure2 = figure('Color',[1 1 1]);                    % Plot raw data

box('on');  hold('all'); %ylim([98.9 99.2]);grid('on');
plot(temp2D(:,1),temp2D(:,tr));
plot(T,temp2D(:,tr),'Color',1/255*[0 0 255]);
plot(T,mean(temp2D(:,tr)),'-r');
xlabel ('Time [S]','FontSize',12,'FontName','Calibri');
ylabel ('Pressure [-]','FontSize',12,'FontName','Calibri');
title('Prototype 50% load','FontSize',14,'FontName','Calibri');
xlim([0,0.2]);

%%
%finner topp- og bunnpunkt
%sett begrensing på hvilke ekstempunkter som tas med
%plotter gjennomsnitt av ekstrempunkter og generell mean

trykk=temp2D(:,tr);
```

```
[pksThr,locsThr] = findpeaks(trykk,'minpeakdistance',9);%,'minpeakheight',2.8);

mintrykk=-1*trykk;
[pksThrmin,locsThrmin] = findpeaks(mintrykk,'minpeakdistance',9);%,'minpeakheight',-2.6);

figure(3)
plot(T,trykk, T(locsThr),pksThr,'rv','MarkerFaceColor','r');  hold on
plot(T,trykk, T(locsThrmin),-pksThrmin,'rv','MarkerFaceColor','r');  hold on
plot(T,mean(pksThr),'-r');
plot(T,-mean(pksThrmin),'-r');
plot(T,mean(trykk));
set(gcf,'color','w');
xlabel ('Time [S]','FontSize',12,'FontName','Calibri');
ylabel ('Pressure [-]','FontSize',12,'FontName','Calibri');
title('Time','FontSize',14,'FontName','Calibri');
xlim([0,0.5]);
%ylim([2,4]);


%%

%plotter scatter amplitude
last=[42 50 75];

amplitudeP= mean(pksThr)+mean(pksThrmin);
y=3;
load=last(1,OP);
zoom=1000;


figure(4)
scatter(load,y,zoom*amplitudeP,'filled','b'); hold on;

xlim([20,100]);
ylim([0,4]);

xlabel ('Load [%]','FontSize',12,'FontName','Calibri');
set(gca,'YTickLabel', {'Prototype/Model', 'Model', 'Prototype'}, 'YTick',[1 2 3]);
title('Comparison','FontSize',14,'FontName','Calibri')

ampl(1,OP)=amplitudeP;



%clearvars -except Runnermat amplitude pksThr pksThrmin ampl
```

```
%% Tar inn data og velger kolonner som skal samples
clearvars -except cal data amplM
clc
load('caldata.mat');
Col=[1 2 3 4 5 6 7 8];
HM=35.45;

c=[1 2 3 10];       %stasjonær
d=[1 2 3];          %roterende
samp=2;             %antall samp. pluss 1
tr=2;               %velger hva man vil se på
op=3;               %velger driftspunkt
OPN=3;

temp2D(:,1:4)=data{op,1}(:,c);
temp2D(:,5:7)=data{op,samp}(:,d);

ncolumns=7;
nsamples=29999;
exlim=30;           %setter xaksen

%% Normaliserer resultatene.

for i=1:ncolumns
    temp2D_rms(:,i)=temp2D(:,i)-rms(temp2D(:,i));
end



Fs=2000;
nfft=nsamples;
L=floor(nfft/2+1);

pwelchArray2D=zeros(L,3);
pwelchArray3D=zeros(L,3,ncolumns);
y=zeros(L,1);
T=(0:1:nfft-1)/Fs;


window_weight=(L/2);
overlapPercent=70;

for i=1:ncolumns
    [pxx,f] = pwelch(temp2D_rms(:,i), hanning(window_weight),overlapPercent, nfft,Fs);

    for j=1:L
     y(j)=Col(:,i);

    end

 pwelchArray2D=[f y pxx];
 pwelchArray3D(:,:,i)=(pwelchArray2D);

end

g=pwelchArray3D(:,1,tr);
h=pwelchArray3D(:,3,tr);
```

```
for i=1:ncolumns
    temp2D(:,i)=temp2D(:,i)./HM;
end
%% Plotter resultatene

Fig=figure('Color',[1 1 1]);

box('on');hold('all');
  xlim([0,exlim]);
  grid on
dcm_obj = datacursormode(Fig);
set(dcm_obj,'UpdateFcn',@display_data,'DisplayStyle','datatip','SnapToDataVertex','off',
'Enable','on')
stem(g./9,h./HM,'Marker','none','Color',1/255*[0 0 255]);
xlabel ('Frequency [-]','FontSize',12,'FontName','Calibri');
ylabel ('Amplitude [-]','FontSize',12,'FontName','Calibri');
title('Model 50% load','FontSize',14,'FontName','Calibri');
xlim([0,1.2])

figure2 = figure('Color',[1 1 1]);

% Plot raw data
box('on');  hold('all');

plot(T,temp2D(:,tr),'Color',1/255*[0 0 255]);
plot(T,mean(temp2D(:,tr)),'-r');
xlabel ('Time [S]','FontSize',12,'FontName','Calibri');
ylabel ('Pressure [-]','FontSize',12,'FontName','Calibri');
title('Model 50% load','FontSize',14,'FontName','Calibri')
xlim([0,5]);

%%
trykk=temp2D(:,tr);

[pksThrM,locsThrM] = findpeaks(trykk,'minpeakdistance',100);

mintrykk=-1*trykk;
[pksThrminM,locsThrminM] = findpeaks(mintrykk,'minpeakdistance',100);

figure(3)
plot(T,trykk, T(locsThrM),pksThrM,'rv','MarkerFaceColor','r');  hold on
plot(T,trykk, T(locsThrminM),-pksThrminM,'rv','MarkerFaceColor','r');  hold on
plot(T,mean(pksThrM),'-r');
plot(T,-mean(pksThrminM),'-r');
plot(T,mean(trykk));
set(gcf,'color','w');
xlim([0,5]);

%%
last=[42 50 75];

amplitudeM= mean(pksThrM)+mean(pksThrminM);
y=2;
load=last(1,OPN);
zoom=1000;
```

```
figure(4)
scatter(load,y,zoom*amplitudeM,'filled','b'); hold on;

xlim([20,100]);
ylim([0,4]);

xlabel ('Load [%]','FontSize',12,'FontName','Calibri');
set(gca,'YTickLabel', {'Prototype/Model', 'Model', 'Prototype'}, 'YTick',[1 2 3]);
title('Comparison','FontSize',14,'FontName','Calibri')

amplM(1,OPN)=amplitudeM;

%clearvars -except amplM
```

```
%% IMPORT rådata fra tester inn i MATLAB.
%Viktig å ikke ha noen excelfiler oppe når man kjører da dette vil påvirke
%variabelen length.

%Leser excelfiler med navn stasjAA_BB.xlsx hvor AA angir målepunkt og BB
%angir de gjentatte målingene.

clear all
clc
%Kjører samme punkt et visst antall ganger, legger disse under hverandre i
%matrisen.

%% DATA IMPORT ----------------------------------------------------------
% Strukturerer data i  matrisen cal.

nindsamp=1;                         %setter inn antall rep av et operasjonspunkt
mappe= uigetdir;
filepattern=strcat(mappe,'\*.xlsx');
% filepattern=fullfile('M:','MATLAB','Resultat','*.xlsx');
xlsxfiles=dir(filepattern);
length=(length(xlsxfiles))/(2*nindsamp)-2;   %Angir antall punkter målt

xlrange1='A3:M30001';
xlrange2='A3:Y30001';


for k = 1:length
    for h=1:nindsamp              %endres til antall uavhengige triggerpunkter

        xlfilename1 = sprintf('stasj%d_%d.xlsx', k,h);
        xlfilename2 = sprintf('rot%d_%d.xlsx', k,h);
        cal{k,h}=xlsread(strcat(mappe,'\',xlfilename1),2,xlrange1);
        cal{k,h+nindsamp}=xlsread(strcat(mappe,'\',xlfilename2),2,xlrange2);

    end
end

%%   Finner antall filer og lager hovedmatrisen (3D) masterarray.

nsamples=(30001-3)*length;


%b=[1 5 6 10 11 12 13 18 19 22 25] ; %Luker ut de ødelagte trykksensorene fra matrisen.
b=[1 12 25];

for k=1:length
    for h=1:nindsamp
        cal{k,h+nindsamp}=cal{k,h+nindsamp}(:,b);
    end
end

c=[1 2 3 4 5 6 7 8 9 10 11 13];

for k=1:length
    for h=1:nindsamp
        cal{k,h}=cal{k,h}(:,c);
    end
```

```
end



clearvars -except cal
save('Data') %lagrer cal i Data.mat. NB skriver over eventuelle tidligere filer med samme
navn.

%Ex for å hente opp en kolonne fra cal: cal{1,2}(:,5); henter opp
%kolonne 5 fra roterende RIO, punkt 1.

%%
%
%
%
% for i=1:14
%     for j=2:7
% plot(RunnerProto{i}(:,1),RunnerProto{i}(:,j)), hold on;
%
%     end
%end
```

Risikovurderingsrapport

Francisriggen

Prosjekttittel	Modelltest
Prosjektleder	Torbjørn K. Nielsen
Enhet	NTNU
HMS-koordinator	Erik Langørgen
Linjeleder	Olav Bolland
Plassering	Vannkraftlaboratoriet
Romnummer	42
Riggansvarlig	Ingeborg L. Bue og Julie M. Hovland
Risikovurdering utført av	Ingeborg L. Bue og Julie M. Hovland

TABLE OF CONTENTS

1 INTRODUCTION

Description of experiment setup and the purpose of the experiments. Where is the rig located?

2 ORGANISATION

Rolle	NTNU	Sintef
Lab Ansvarlig:	Morten Grønli	Harald Mæhlum
Linjeleder:	Olav Bolland	Mona Mølnvik
HMS ansvarlig: HMS koordinator HMS koordinator	Olav Bolland Erik Langørgen Bård Brandåstrø	Mona Mølnvik Harald Mæhlum
Romansvarlig:	Bård Brandåstrø	
Prosjekt leder:	Torbjørn Nielsen	
Ansvarlig riggoperatører:	Ingeborg L. Bue og Julie M. Hovland	

3 RISK MANAGEMENT IN THE PROJECT

Hovedaktiviteter risikostyring	Nødvendige tiltak, dokumentasjon	DATE
Prosjekt initiering	Prosjekt initiering mal	
Veiledningsmøte Guidance Meeting	Skjema for Veiledningsmøte med pre-risikovurdering	
Innledende risikovurdering Initial Assessment	Fareidentifikasjon – HAZID Skjema grovanalyse	
Vurdering av teknisk sikkerhet Evaluation of technical security	Prosess-HAZOP Tekniske dokumentasjoner	
Vurdering av operasjonell sikkerhet Evaluation of operational safety	Prosedyre-HAZOP Opplæringsplan for operatører	
Sluttvurdering, kvalitetssikring Final assessment, quality assurance	Uavhengig kontroll Utstedelse av apparaturkort Utstedelse av forsøk pågår kort	

4 DRAWINGS, PHOTOS, DESCRIPTIONS OF TEST SETUP

Attachments:
Process and Instrumentation Diagram (PID)
Shall contain all components in the experimental setup
Component List with specifications
Drawings and photos describing the setup.
Where the operator is present, how is the gas bottles, shutdown valves for water / air.

5 EVACUATION FROM THE EXPERIMENT AREA

Evacuate at signal from the alarm system or local gas alarms with its own local alert with sound and light outside the room in question, see 6.2
Evacuation from the rigging area takes place through the marked emergency exits to

the assembly point, (corner of Old Chemistry Kjelhuset or parking 1a-b.)
Action on rig before evacuation:
(Shut off the air and water supply. Power off the electrical supply.)

6 WARNING

6.1 Before experiments

E-mail with information about the planned experiment to: iept-experiments@ivt.ntnu.no
The e-mail should contain the following items:

- Name of responsible person:
- Experimental setup/rig:
- Start Experiments: (date and time)
- Stop Experiments: (date and time)

You should get the approval back from the laboratory management before start up. All running experiments are notified in the activity calendar for the lab to be sure they are coordinated with other activity.

6.2 Nonconformance

FIRE
Fire you are not able to put out with locally available fire extinguishers, activate, the nearest fire alarm and evacuate area. Be then available for fire brigade and building caretaker to detect fire place.
If possible, notify:

NTNU	SINTEF
Labsjef Morten Grønli, tlf: 918 97 515	Labsjef Harald Mæhlum, : tlf 930 149 86
HMS: Morten Grønli, tlf: 918 97 515 HMS: Per Bjørnaas , tlf: 91897123	Forskningssjef Mona Mølnvik
Instituttleder: Olav Bolland: 91897209	
NTNU Sintef Beredskapstelefon	800 80 388

GASALARM
At a gas alarm, close gas bottles immediately and ventilated the area. If the level of gas concentration not decrease within a reasonable time, activate the fire alarm and evacuate the lab. Designated personnel or fire department checks the leak to determine whether it is possible to seal the leak and ventilate the area in a responsible manner.
Alert Order in the above paragraph.

PERSONAL INJURY

- First aid kit in the fire / first aid stations
- , Shout for help
- Start life-saving first aid•

CALL 113 if there is any doubt whether there is a serious injury

Other Nonconformance (AVVIK)
NTNU:
Reporting nonconformance, Innsida, avviksmelding:
https://innsida.ntnu.no/lenkesamling_vis.php?katid=1398
SINTEF:
Synergi

7 ASSESSMENT OF TECHNICAL SAFETY

7.1 HAZOP

See Chapter 13 "Guide to the report template".

The experiment set up is divided into the following nodes:

Node 1	Pipe system with pump
Node 2	Rotating turbine/shaft with mounted hardware
Node 3	Hydraulics

Attachments:, skjema: Hazop

Conclusion:

Vurdering:

Node1:

-Overtrykksventil som slår ut dersom trykket i systemet blir for høyt.

-Rørelementer er eksternt levert og godkjent for aktuelt trykk.

Node2:

-Roterende utstyr står utilgjengelig for folk. Dvs det er innkapslet eller man må klatre for å nå opp til det.

Node3:

-Trykk i slanger og rør(olje vann) Hydraulikkslanger er ikke egenprodusert, men trykksatt

-Trykksatt utstyr er sertifisert og kjøpt inn av eksterne leverandører med god kompetanse

7.2 Flammable, reactive and pressurized substances and gas

Contains the experiments Flammable, reactive and pressurized substances and gas

JA	Trykksatt hydraulikkolje, trykksatt vann

Attachments:

Conclusion: Arbeidsmedium er vann. Alle rør er levert av eksternt firma med prøvesertifikat Hydraulikk til hydrostatisk lager. Hyllevare komponenter, de er dermed ikke egenprodusert.

7.3 Pressurized equipment

Contain the set up pressurized equipment?

JA	Utstyret trykktestes i henhold til norm og dokumenteres

Attachments:

Conclusion*:* Prøvesertifikat for trykktesting finnes i labperm.

7.4 Effects on the environment (emissions, noise, temperature, vibration, smell)

NEI	

Conclusion:

7.5 Radiation

See Chapter 13 "Guide to the report template".

NEI	

Attachments:

Conclusion:

7.6 Usage and handling of chemicals.

See Chapter 13 "Guide to the report template".

JA	

Attachments: MSDS
Conclusion: Hydraulikkolje, mineralsk olje. Datablad er vedlagt.

7.7 El safety (need to deviate from the current regulations and standards.)

NEI	

Attachments:
Conclusion: Alt elektrisk utstyr er forsvarlig montert og står slik permanent.

8 ASSESSMENT OF OPERATIONAL SAFETY

For ensuring that established procedures cover all identified risk factors that must be taken care of through procedures and ensure that the operators and technical performance have sufficient expertise.

8.1 Prosedure HAZOP

See Chapter 13 "Guide to the report template".
The method is a procedure to identify causes and sources of danger to operational problems.
Attachments: HAZOP_MAL_Prosedyre
Conclusion: Operatør har et eget rom for å kjøre riggen.

8.2 Operation and emergency shutdown procedure

See Chapter 13 "Guide to the report template".
The operating procedure is a checklist that must be filled out for each experiment.
Emergency procedure should attempt to set the experiment set up in a harmless state by unforeseen events.
Attachments: Procedure for running experiments
Emergency shutdown procedure: Nødstopp i kontrollrom.

8.3 Training of operators

A Document showing training plan for operators

- Kjøring av pumpesystem.

Vedlegg: Opplæringsplan for operatører

8.4 Technical modifications

- Technical modifications made by the Operator
  o None
- • Technical modifications that must be made by Technical staff:
  o Everything
- • What technical modifications give a need for a new risk assessment; (by changing the risk picture)?

Conclusion: Modifikasjoner gjøres i samråd med Torbjørn Nielsen/Bård Brandåstrø

8.5 Personal protective equipment

- It is mandatory use of eye protection in the rig zone

Conclusion: Vernebriller viktig, pga vann og hydraulikkolje under trykk.

8.5.1 General Safety

Conclusion: Alle forsøk kjøres med operatør til stede og en fast ansatt tilgjengelig på vannkraftlaboratoriet.

8.6 Safety equipment

- Vernebriller

8.7 Special actions

9 QUANTIFYING OF RISK - RISK MATRIX

See Chapter 13 "Guide to the report template".
The risk matrix will provide visualization and an overview of activity risks so that management and users get the most complete picture of risk factors.

IDnr	Aktivitet-hendelse	Frekv-Sans	Kons	RV
1	Lekkasje i Hydraulikk	1	A	A1
2	Fremmedlegemer i vannet	1	A	A1
3	Rørbrudd	1	A	A1
4	Roterende Aksling	1	B	B1
5	Roterende festebrakett med hardware	1	A	A1

Conclusion : *Det er liten restrisiko ved forsøkene, foruten at trykksatt vann og olje fordrer bruk av vernebriller. Fremmedlegemer i vannet gir liten risiko for personskade, men kan føre til store skader på maskineri.*

10 CONCLUSJON

Riggen er bygget til god laboratorium praksis (GLP).

Hvilke tekniske endringer av driftsparametere
vil kreve ny risikovurdering:

Komponent mot komponent krever ikke. Ellers må ny risikovurdering utføres.

Apparaturkortet får en gyldighet på **4 måneder.**
Forsøk pågår kort får en gyldighet på **4 måneder**.

11 REGULATIONS AND GUIDELINES

Se http://www.arbeidstilsynet.no/regelverk/index.html

- Lov om tilsyn med elektriske anlegg og elektrisk utstyr (1929)
- Arbeidsmiljøloven
- Forskrift om systematisk helse-, miljø- og sikkerhetsarbeid (HMS Internkontrollforskrift)
- Forskrift om sikkerhet ved arbeid og drift av elektriske anlegg (FSE 2006)
- Forskrift om elektriske forsyningsanlegg (FEF 2006)
- Forskrift om utstyr og sikkerhetssystem til bruk i eksplosjonsfarlig område NEK 420
- Forskrift om håndtering av brannfarlig, reaksjonsfarlig og trykksatt stoff samt utstyr og anlegg som benyttes ved håndteringen
- Forskrift om Håndtering av eksplosjonsfarlig stoff
- Forskrift om bruk av arbeidsutstyr.
- Forskrift om Arbeidsplasser og arbeidslokaler
- Forskrift om Bruk av personlig verneutstyr på arbeidsplassen
- Forskrift om Helse og sikkerhet i eksplosjonsfarlige atmosfærer
- Forskrift om Høytrykksspyling
- Forskrift om Maskiner
- Forskrift om Sikkerhetsskilting og signalgivning på arbeidsplassen
- Forskrift om Stillaser, stiger og arbeid på tak m.m.
- Forskrift om Sveising, termisk skjæring, termisk sprøyting, kullbuemeisling, lodding og sliping (varmt arbeid)
- Forskrift om Tekniske innretninger
- Forskrift om Tungt og ensformig arbeid
- Forskrift om Vern mot eksponering for kjemikalier på arbeidsplassen (Kjemikalieforskriften)
- Forskrift om Vern mot kunstig optisk stråling på arbeidsplassen
- Forskrift om Vern mot mekaniske vibrasjoner
- Forskrift om Vern mot støy på arbeidsplassen

Veiledninger fra arbeidstilsynet
se: http://www.arbeidstilsynet.no/regelverk/veiledninger.html

12 DOCUMENTATION

- Tegninger, foto, beskrivelser av forsøksoppsetningen
- Hazop_mal
- Sertifikat for trykkpåkjent utstyr
- Håndtering avfall i NTNU
- Sikker bruk av LASERE, retningslinje
- HAZOP_MAL_Prosedyre
- Forsøksprosedyre
- Opplæringsplan for operatører
- Skjema for sikker jobb analyse, (SJA)
- Apparaturkortet
- Forsøk pågår kort

13 GUIDANCE TO RISK ASSESSMENT TEMPLATE

Kap 7 Assessment of technical safety.

Ensure that the design of the experiment set up is optimized in terms of technical safety. Identifying risk factors related to the selected design, and possibly to initiate re-design to ensure that risk is eliminated as much as possible through technical security.

This should describe what the experimental setup actually are able to manage and acceptance for emission.

7.1 HAZOP

The experimental set up is divided into nodes (eg motor unit, pump unit, cooling unit.). By using guidewords to identify causes, consequences and safeguards, recommendations and conclusions are made according to if necessary safety is obtained. When actions are performed the HAZOP is completed.

(e.g. "No flow", cause: the pipe is deformed, consequence: pump runs hot, precaution: measurement of flow with a link to the emergency or if the consequence is not critical used manual monitoring and are written into the operational procedure.)

7.2 Flammable, reactive and pressurized substances and gas.

According to the Regulations for handling of flammable, reactive and pressurized substances and equipment and facilities used for this:

Flammable material: Solid, liquid or gaseous substance, preparation, and substance with occurrence or combination of these conditions, by its flash point, contact with other substances, pressure, temperature or other chemical properties represent a danger of fire.
Reactive substances: Solid, liquid, or gaseous substances, preparations and substances that occur in combinations of these conditions, which on contact with water, by its pressure, temperature or chemical conditions, represents a potentially dangerous reaction, explosion or release of hazardous gas, steam, dust or fog.
Pressurized : Other solid, liquid or gaseous substance or mixes havinig fire or hazardous material response, when under pressure, and thus may represent a risk of uncontrolled emissions

Further criteria for the classification of flammable, reactive and pressurized substances are set out in Annex 1 of the Guide to the Regulations "Flammable, reactive and pressurized substances"
http://www.dsb.no/Global/Publikasjoner/2009/Veiledning/Generell%20veiledning.pdf
http://www.dsb.no/Global/Publikasjoner/2010/Tema/Temaveiledning_bruk_av_farlig_stoff_Del_1.pdf

Experiment setup area should be reviewed with respect to the assessment of Ex zone

- Zone 0: Always explosive atmosphere, such as inside the tank with gas, flammable liquid.
- Zone 1: Primary zone, sometimes explosive atmosphere such as a complete drain point
- Zone 2: secondary discharge could cause an explosive atmosphere by accident, such as flanges, valves and connection points

7.4 Effects on the environment

With pollution means: bringing solids, liquid or gas to air, water or ground, noise and vibrations, influence of temperature that may cause damage or inconvenience effect to the environment.
Regulations: http://www.lovdata.no/all/hl-19810313-006.html#6
NTNU guidance to handling of waste:http://www.ntnu.no/hms/retningslinjer/HMSR18B.pdf

7.5 Radiation

Definition of radiation

Ionizing radiation: Electromagnetic radiation (in radiation issues with wawelength <100 nm) or rapid atomic particles (e.g. alpha and beta particles) with the ability to stream ionized atoms or molecules.
Non ionizing radiation: Electromagnetic radiation (wavelength >100 nm), og ultrasound$_1$ with small or no capability to ionize.
Radiation sources: All ionizing and powerful non-ionizing radiation sources.
Ionizing radiation sources: Sources giving ionizing radiation e.g. all types of radiation sources, x-ray, and electron microscopes.
Powerful non ionizing radiation sources: Sources giving powerful non ionizing radiation which can harm health and/or environment, e.g. class 3B and 4. MR$_2$ systems, UVC$_3$ sources, powerful IR sources$_4$.
$_1$Ultrasound is an acoustic radiation ("sound") over the audible frequency range (> 20 kHz). In radiation protection regulations are referred to ultrasound with electromagnetic non-ionizing radiation. $_2$MR (e.g. NMR) - nuclear magnetic resonance method that is used to "depict" inner structures of different materials. $_3$UVC is electromagnetic radiation in the wavelength range 100-280 nm. $_4$IR is electromagnetic radiation in the wavelength range 700 nm - 1 mm.

For each laser there should be an information binder (HMSRV3404B) which shall include:

- General information
- Name of the instrument manager, deputy, and local radiation protection coordinator
- Key data on the apparatus
- Instrument-specific documentation
- References to (or copies of) data sheets, radiation protection regulations, etc.
- Assessments of risk factors
- Instructions for users